Thesis of the degree of Doctor of Philosophy in Science

ELECTRONIC AND OPTICAL PROPERTIES OF THREE DIMENSIONAL CHARGE DENSITY WAVE SYSTEM IN $BaBiO_3$

S. M. Hasanuzzaman

March 24, 1999

Department of Synchrotron Radiation Science,
School of Mathematical and Physical Science,
The Graduate University for Advanced Studies,
Kanagawa, Hayama, JAPAN.

This Doctoral thesis is quoted from the following papers:

1. " Theory for Optical Absorption, Direct and Indirect Excitons in $BaBiO_3$ " S. M. Hasanuzzaman, Kaoru Iwano and Keiichiro Nasu. *J. Phys. Soc. Jpn.* **68** (1999), No. 4.
2. " Nonlinear excitations in charge- and spin-density-wave materials-, excitons, solitons and (bi)polarons " K. Iwano, S. M. Hasanuzzaman, N. Tomita and K. Nasu. **To be published in *Synth. Met.*** 1999.

CONTENTS

Pages

1. INTRODUCTION

Since the advent of high-T_c superconductivity in copper oxides by Bednorz and Müller [1], the interest in solid state properties of various oxides such as Cu-oxides, Bi-oxides, Mn-oxides and Ti-oxides, has been widely renewed. In these metal oxides the various noble properties are said to come from the strong inter-electron coulombic correlation and (or) the strong electron-lattice coupling. Among those materials, $BaBiO_3$ (BBO) and its related compounds $BaPb_{1-x}Bi_xO_3$ (BPBO) and $Ba_{1-x}K_xBiO_3$ (BKBO), are the objects of a special interest. $BaBiO_3$ becomes a superconductor if doped with Pb at the Bi sites (with a maximum of T_c~12 K for x~0.25) [2], and also shows superconductivity if it is doped with K at the Ba sites (with a maximum of T_c~30 K for x~0.40) [3]. In these materials, the strong electron-phonon (el-ph) coupling is inferred to play very important roles, and we will focus on this coupling. It can give two properties, one is superconductivity and other is charge density wave (CDW) type insulator. The very strong el-ph coupling will give two instabilities. If the whole system remains in the metallic state, it will give high-T_c superconductor. However, it also causes a structural instability like CDW state. So, these two basic possibilities come from el-ph coupling. In order to clarify such a strong el-ph coupling, which gives CDW, it is necessary to understand how electron couples with phonon, and how it effects on the ground state as well as various excited states therefrom.

In spite of this renewed interest, the basic electronic structure of the parent material $BaBiO_3$ is still not clarified sufficiently. These material present several peculiarities with comparing to other perovskite type high-T_c superconductor compounds. It is a three dimensional system, does not contain any magnetic ions and absence of two dimensional metal-oxygen plane. In the undoped phase of

this material, a static charge density wave state with a periodic lattice distortion appears, opens up a gap at the Fermi level, and makes this compound a Peierls insulator. Furthermore, the superconductivity appears when this CDW order is destroyed by doping.

From the band structure calculation for cubic (hypothetical metallic) $BaBiO_3$, the Fermi level is expected to lie just in the middle of a broad conduction band, that arises from strong hybridization between Bi 6s and O 2p orbitals [4]. Since the average valence of Bi in $BaBiO_3$ is 4^+, the electronic configuration of Bi^{4+} would be $5d^{10}6s^1$. With its unpaired 6s electron, such an ion is expected to be paramagnetic, and the compound would be metallic due to the half-filled broad conduction band. However, experimentally, the compound is diamagnetic. Although, the band structure calculations predict a metallic behavior for $BaBiO_3$ [4,5,6], experimental works [7,8] show that the material is an insulator.

To solve this problem, the Bi charge disproportionation into Bi^{3+} and Bi^{5+} configurations is generally considered, thus skipping up the intermediate valence 4^+ [8]. In reality, Bi_2O_3 and Bi_2O_5 compounds do exist, BiO_2 does not exist. If this situation prevails, several properties are expected to be derived from the disproportionation. (i) Since Bi^{3+} and Bi^{5+} have different ionic radii (1.03 and 0.76 $\mathring{A}$, respectively, in octahedral configuration) [9], two different Bi-O distances are expected. (ii) The opening of gaps at the Fermi level is also expected. (iii) A structural change from the simple perovskite structure is expected to occur because of two Bi-O distances. The bismuth disproportionation has been discussed in terms of a charge density wave instability by many authors [10,11]. This CDW may open a gap at the Fermi surface, and is consistent with the observed insulating character of $BaBiO_3$. Other experimental data also seem to be consistent with this picture. That is, X-

ray diffraction indicates a monoclinic distortion from the simple cubic perovskite. Neutron diffraction experiments [12] also reported two different Bi-O distances, viz., 2.28 $\mathring{A}$ and 2.12 $\mathring{A}$, as confirmed by Thornton and Jacobson [13].

However, a fundamental question is, what are the electronic states or the band structure of this material? The band structure calculated by Mattheiss and Hamann [4] with the linearized augmented plane wave (LAPW) method well explains most of the properties of the metallic phase, but does not work so well in the insulating phase or in the metal-insulator (MI) transition region. According to their CDW like image, the energy gap can appear only near x=1.0, whereas insulating properties have been observed to persist over a wide range: $0.35 < x \leq 1.0$. Rice and Sneddon [14] interpreted the semiconductivity of BBO as due to the real-space electron pairing which gives rise to the valence configuration $Ba_2Bi^{3+}Bi^{5+}O_3$. They concluded that the MI transition takes place as Pb dilutes the $Bi^{3+} - Bi^{5+}$ superlattice and weakens the real- space pairing [15]. Yoshioka and Fukuyama [16] considered a negative U Hubbard model with on-site disorder for the bismuthates. They believed that, in BPBO, there is no metal semiconductor transition but only a transition from a semiconductor to a superconductor (at T=0 K). But there is no firm experimental evidence for it. Recent density functional theory calculations [17] for breathing distorted BBO indicated that the U values of Bi are positive and there is no evidence for a negative U at Bi atoms. Electron diffraction study of the structural transitions in BPBO has been performed on powder samples by Koyama and Ishimara [18], and Minami [19]. The phase diagram as a function of doping (x) that Koyama and Ishimara obtained is different from the one reported by Cox and Sleight [12] earlier. They found evidence for tetragonal and monoclinic phases at low temperature and a cubic phase at high temperature.

They have investigated the non existence of incommensurate phase, in agreement with Cox and Sleight.

A number of theoretical studies [4,20-22], and experimental measurements [7,23-29] have been performed in order to investigate the band structure, as well as the optical properties of this parent material $BaBiO_3$. Using the local density approximation, Liechtenstein *et al.* [21] have shown that a gap opens up between the split Bi 6s sub-bands. They found a direct gap ($\equiv E_d$) of about 1.3 eV, and an indirect gap ($\equiv E_i$) of about 0.3 eV. While, recent photoemission and x-ray absorption studies by Namatame *et al.* [23], showed that $E_d \approx 1.9$ eV. The existence of the indirect gap was firstly proposed by Uwe and Tachibana from their infrared absorption measurements [24,25]. They estimated the indirect gap E_i of about 0.5 eV, which is much smaller than the direct gap E_d of about 2.0 eV observed in the absorption spectrum of the visible region [7,26]. Very recently, Kim *et al.* [27] have also measured the absorption spectrum and estimated the indirect gap E_i as 0.84 eV. Thus, we have seen that there are many different and mutually conflicting proposals for the electronic excitations in the infrared and visible regions of $BaBiO_3$.

Raman experiments [28,29] on $BaBiO_3$ show the resonant enhancement and appearance of higher harmonics of the 570 cm^{-1} phonon mode (breathing mode). This indicates that the optical gap is closely related to the strong electron phonon interaction in the system [28,30,]. Inoue *et al.* [31] have reported the infrared activeness of the Bi-Bi stretching mode, which is one of the direct evidence for the charge disproportionation between Bi sites.

As is well known, there are many insulators which show both direct and indirect optical transitions [32]. In usual insulators, however, the opening of optical gap (direct gap) and the appearance of indirect gap are often considered separately. The optical gap usually comes from the difference between the

occupied and unoccupied atomic orbitals relevant to the valence and the conduction bands. While the indirect transition usually appears because of the weak electron-phonon coupling, which slightly mixes up direct and indirect transitions.

On the other hand, it is inferred that a strong electron-phonon interaction, acting in this present material $BaBiO_3$, causes a Peierls distortion of the lattice, doubling the unit cell, opening up a wide direct gap, and also makes the indirect transition to appear. So both the direct gap and the appearance of the indirect transition have the same origin. For this reason, in our theory, we will not use the conventional perturbation approach, instead, we will develop a unified theory based on the extended Peierls-Hubbard model.

So, we will see that two types of gap exist in this BBO. One is direct and the other is indirect. Also the appearance of this direct and indirect gaps are due to the characteristic and complicated nature of the one electron energy band $E(k)$ around the Fermi level. Because, in the case of three dimensional metal oxides, the one body energy $E(k)$ of the electron around the Fermi level is usually a complicated function of k. It depends on the nature of three dimensional chemical bonds among the one s-orbital of the metallic atom and the three p-orbitals of O's. As a result, it often occurs that even after the CDW type metal insulator transition, optical excitations appear below the CDW gap. In this case, we have a *mid-gap-absorption*, which is not due to the collective excitations in the gap such as solitons, but simply due to the complicated k-dependency of the one electron energy band. Recently, this type low energy optical excitation is found below the CDW gap of $BaBiO_3$ [33-37].

Photo-induced reflectance measurements [33] of BBO are reported, and several new peaks in the reflectance spectra are observed around the mid-gap energy. This indicates the evidence for a lattice relaxation after removing

electrons from the valence band, and as a consequence, new energy levels appear within the gap, producing mid gap states.

So our purpose, in this present work, is to theoretically clarify the above mentioned optical and electronic properties as well as lattice relaxation of photogenerated excitation in $BaBiO_3$. By using extended Peierls-Hubbard model, we clarify this problem from a unified point of view in connection with the direct and indirect excitons. We will introduce the adiabatic approximation for phonons and the Hartree-Fock approximation for inter-electron coulombic interactions. The electron-hole correlation on the Bi atoms and the classical fluctuation of the oxygen sublattice coordinates are also taken into account, so as to obtain exciton effects as well as thermal fluctuations of the lattice.

The remaining part of this work is organized as follows: In chap. 2, we briefly review present status of our knowledge for the structure and optical properties of $BaBiO_3$. In chap. 3, we explain some theoretical study, and review some experimental evidence of lattice relaxation. In chap. 4, we describe our model, calculation procedure and clarify the metallic and CDW states. In chap. 5, we clarify the direct and indirect excitons from the unified point of view by using our extended Peierls-Hubbard model. In chap. 6, our numerical calculation for nonlinear lattice relaxation will be presented, and origin of photoinduced absorption will be explained. The last chapter is devoted to conclusions.

2. GENERAL PROPERTIES OF $BaBiO_3$

2.1 CRYSTAL STRUCTURE

The crystal structure of Barium Bismuthates ($BaBiO_3$) is a three dimensional perovskite one, as shown in Fig. 2.1. In this structure, Ba atoms occupy the corners of a cubic cell, O atoms are at the face centers, and Bi is at the body center. There are octahedral clusters of O atoms around each Bi atom.

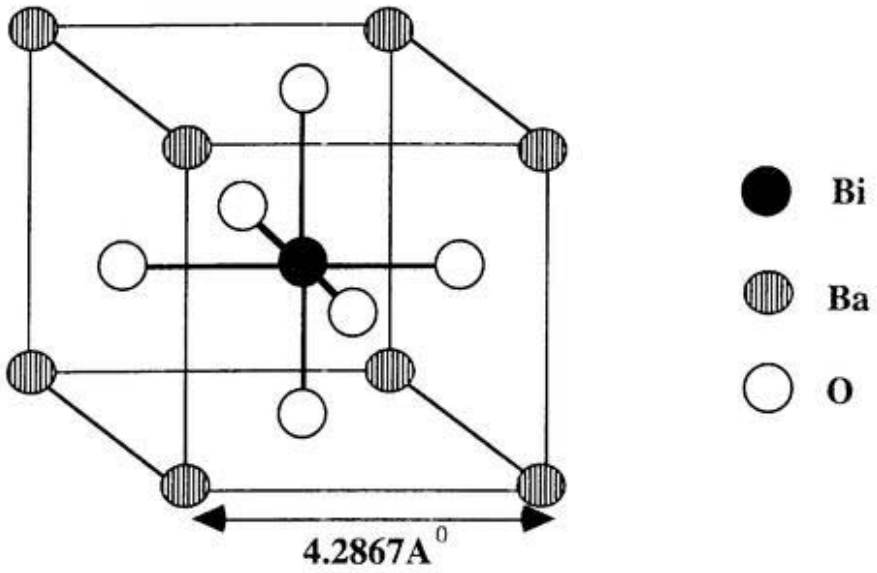

Fig. 2.1. The cubic perovskite crystal structure of $BaBiO_3$.

Slight rotations or breathing mode distortions of these octahedral lead to a variety of non cubic structures. For example, the distortions that yield the pure $BaBiO_3$ structure are shown in Fig. 2.2. Here, there are two distinct nearest neighbor Bi-O distances; 2.28 $\mathring{A}$ and 2.12 $\mathring{A}$. Oxygen octahedra around one of the sublattice cubic structure contract and those around the other sublattice expand, as shown in Fig. 2.3. This can be interpreted in terms of a freezing of the breathing mode of the oxygen octahedra leading to CDW. Such frozen

breathing mode has in fact, been observed in neutron diffraction experiment [38] of BBO.

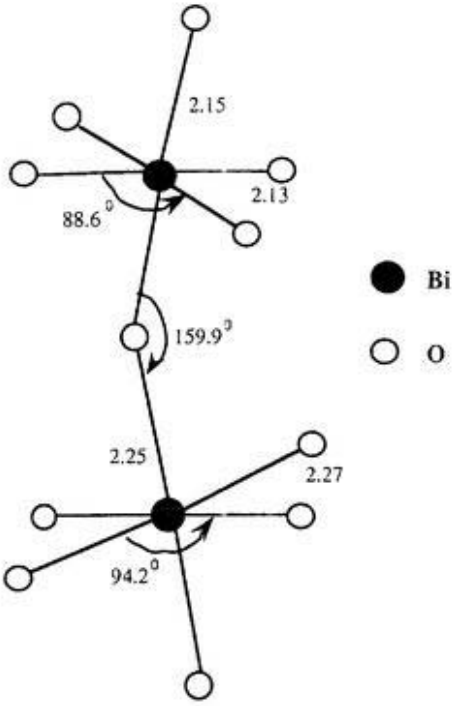

Fig. 2.2. Possible distortions of the cubic perovskite structure. From Ref. [39].

The X-ray and neutron scattering studies of Cox and Sleight [12] determine crystallographic structure of this material. At room temperature, they found that BBO has a periodic but complicated crystalline structure with lattice constant of about 4.2867 $\mathring{A}$.

In the periodic table, Bi is classified in the group V, and the electronic configuration is $1s^2 2s^2 \cdots 5d^{10} 6s^2 6p^3$. It should form compounds with oxidation states 3^+ or 5^+, as these would yield closed outer shell configuration for the corresponding anions. Indeed, these elements generally form compounds with valences 3^+ or 5^+, skipping the intermediate valence 4^+. There are some experimental evidence that Bi charge disproportionation into Bi^{3+} and Bi^{5+} configurations [10,11], thus skipping the intermediate valence 4^+.

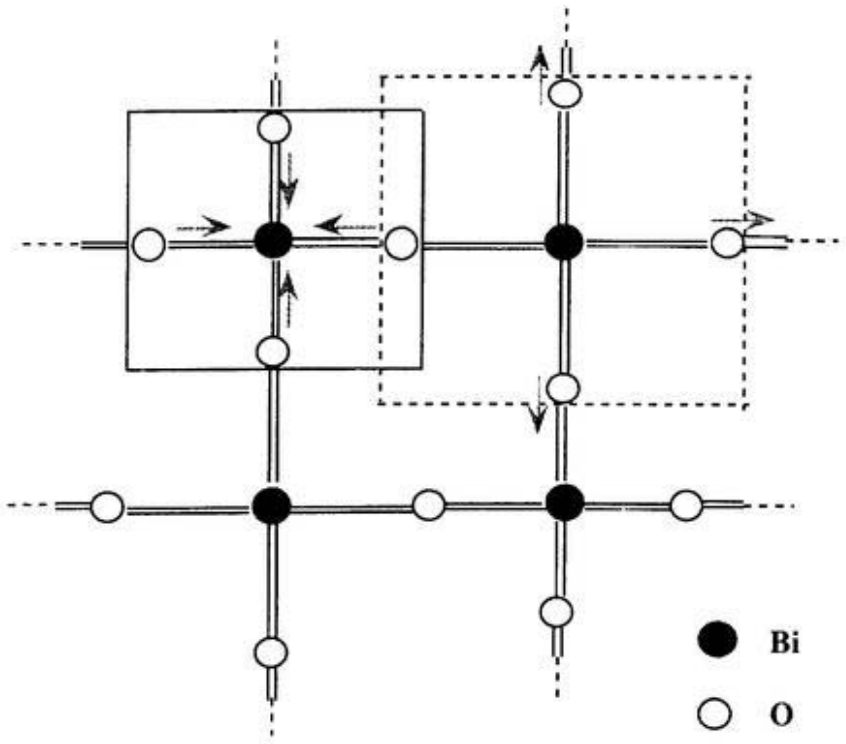

Fig. 2.3(a). Schematic representation of the oxygen octahedra. Only the xy-plane is shown.

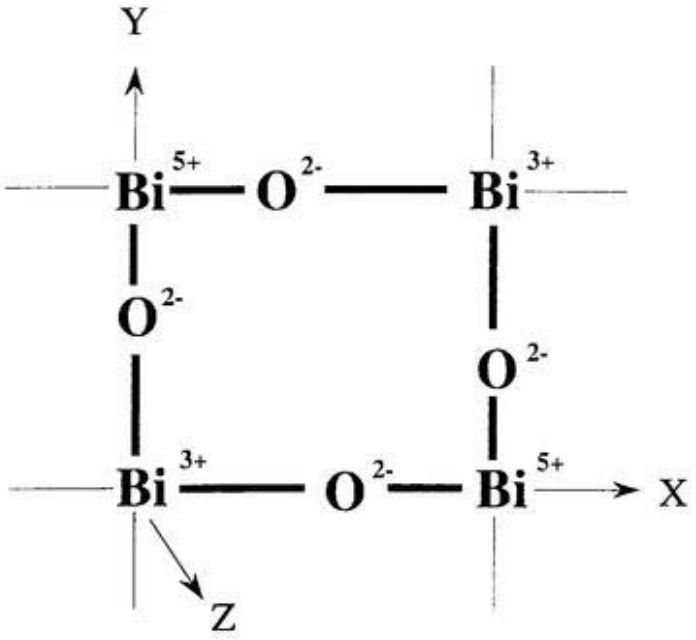

Fig. 2.3(b). Mixed valence state of BiO_6.

There are, in fact , about fifteen elements in the periodic table that shows this extraordinary property of valence skipping. For example, Ge, Sn, and Pb show valences of 2^+ and 4^+, while Ga, In and Tl show 1^+ and 3^+. In all these cases the intermediate valences are either unstable or metastable. The formal valence state of these cations determine the shape and orientation of the other orbitals (of anion) in the compound they form. Hence, any theoretical calculations and predictions of the chemical nature and physical properties of these compounds would necessarily taken into account this information. In addition, the microscopic physics underlying valence skipping is extremely important for the construction of suitable theoretical models.

In an attempt to resolve the valence of Bi, Hair and Blasse [40] concluded that the average valence of Bi is 4^+. In this case, $BaBi^{4+}O_3$ has only one Bi^{4+} ion per unit cell, and this material seems to be metal with a half-filled Bi 6s conduction band. On the other hand, Scholder *et al.* [41] assumed that the oxidation states in BBO are $Ba_2Bi^{3+}Bi^{5+}O_3$, because Bi^{3+} and Bi^{5+} are known to exist in Bi_2O_3 and Bi_2O_5 compounds, respectively.

2.2 PHASE DIAGRAM

The lattice structures that appear in the doped $BaBiO_3$ systems can be viewed as distortions of the basic structure of the simple cubic perovskite shown in Fig. 2.1. The fundamental distortions are tilts of the nominally rigid BiO_6 octahedra, and breathing-mode distortions in which alternating Bi sites become inequivalent because of oxygen-atom displacements toward or away from the Bi atoms. These tilting and breathing-mode distortions can occur independently, or in combination to produce various possible modified perovskite structures. Therefore, both $BaPb_{1-x}Bi_xO_3$ and $Ba_{1-x}K_xBiO_3$

show rich phase diagrams with many structural transitions. Their two dimensional phase diagrams, spanned by temperature T and doping concentration x, are shown schematically in Figs. 2.4 and 2.5, respectively [42,43,44].

In addition to these transitions both bismuthates show metallic, superconducting, and semiconducting phases (Figs. 2.4 and 2.5). The order of these phase transitions are not very clear. The metal-superconductor transitions is, probably, second order. Some works have suggested that there is a first-order transition at finite temperature from the metallic phase to the semiconducting phase [43]. From the available experimental data, it is not clear whether the superconducting and semiconducting phases coexist along any phase boundary and, if so, what are the order of the transition along this boundary is [39,45].

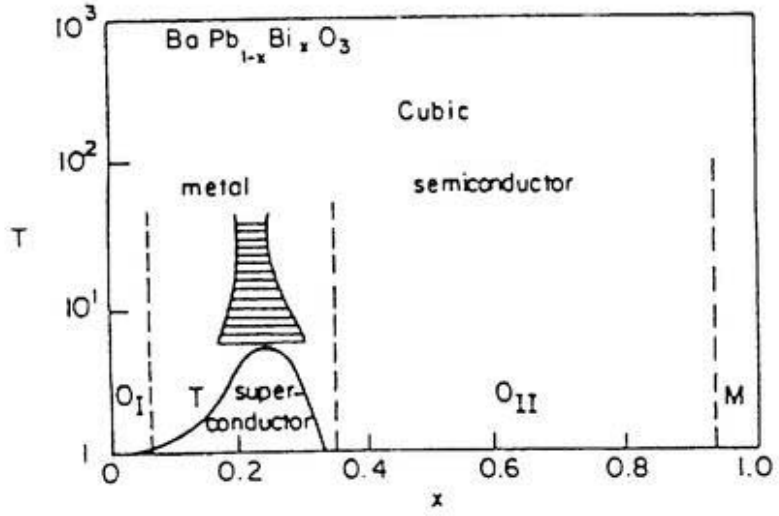

Fig. 2.4. Schematic phase diagram of the BPBO system in the T-x plane. The orthorhombic (O_I) and tetragonal (T) phases are metallic at high temperatures and superconducting at low temperatures. The orthorhombic (O_{II}) and monoclinic (M) phases are semiconducting. From Ref. [43].

However, the maximum value of the superconducting T_c seems to occur at nearly the same value of x as that of the metal-semiconductor transition.

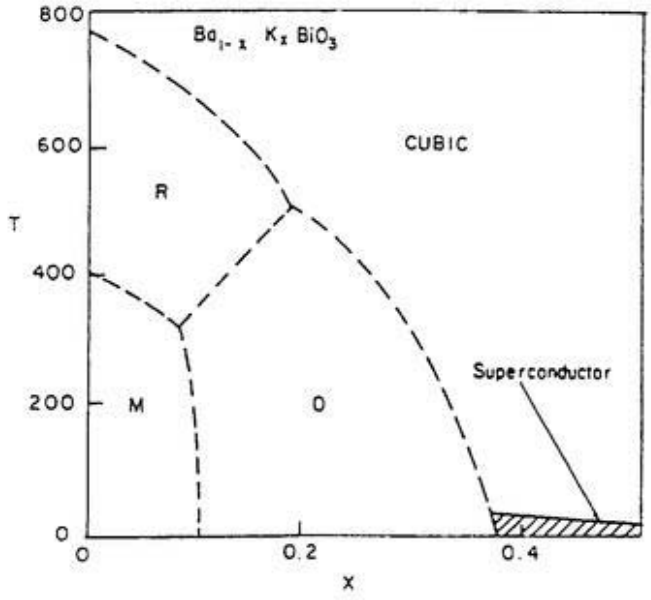

Fig. 2.5. Schematic phase diagram of the BKBO system in the T-x plane. The entire cubic phase is metallic, and the hatched low temperature region is a superconducting phase. The monoclinic (M), orthorhombic (O), and rhombohedral (R) regions are semiconducting. From Ref. [42,46].

Electron diffraction study of the structural transitions in BPBO has been performed on powder samples by Koyama and Ishimara [18], and Minami [19]. The phase diagram as a function of doping (x) that Koyama and Ishimara obtained is different from the one reported by Cox and Sleight [12] earlier. These authors do not get orthorhombic phase in their electron diffraction studies. They found evidence for tetragonal and monoclinic phases at low temperature and a cubic phase at high temperature. They have also investigated the non existence of incommensurate phase and concluded in the negative, in agreement with Cox and Sleight.

In early studies of the lead-doped compound [2] it was suggested that superconductivity could only occur in the tetragonal phase; however, subsequent work seems to suggest that it can also be obtained in specimens with orthorhombic symmetry [45]. On the other hand, in potassium-doped compound, superconductivity has been observed only in the cubic phase [44]. In both the potassium and lead doped systems, the superconducting phase appears right after the semiconductors-metal transition, with increasing lead or potassium concentration.

2.3 ELECTRONIC STRUCTURE

The electronic structure of the $BaBiO_3$ has been studied well using detailed band structure calculations [4,20-22], as well as various experimental methods [28,45,47].

From a theoretical point of view, the electronic band structure calculations for cubic BBO have been carried out by Mattheiss and Hamann [4] on the basis of self consistent linear augmented plane wave (LAPW) method. According to their results, ten complex bands appear in the energy band diagram, as shown in Fig. 2.6. From the electronic configuration of Bi atom, the 4^+ valence state (Bi^{4+}) has an open shell configuration $6s^1$. Each Bi atom is surrounded by six O atoms, which form an octahedron. There are ten orbitals in the unit cell of BiO_3, wherein each O atom contributes three 2p orbitals, and each Bi atom contributes one 6s orbital, as shown in Fig. 2.7. The Bi-O bond lengths are the same for all the six O atoms in the cubic phase. Of the three 2p orbitals at each O atom, one forms σ bond with the Bi 6s orbital, and the rest two form π bonds. The Fermi level crosses the uppermost σ antibonding subband (Fig. 2.6),

leaving it a half-filled metallic band. The electronic conduction mainly occurs through a three dimensional network of this Bi (6s) and O (2p) hybridized state.

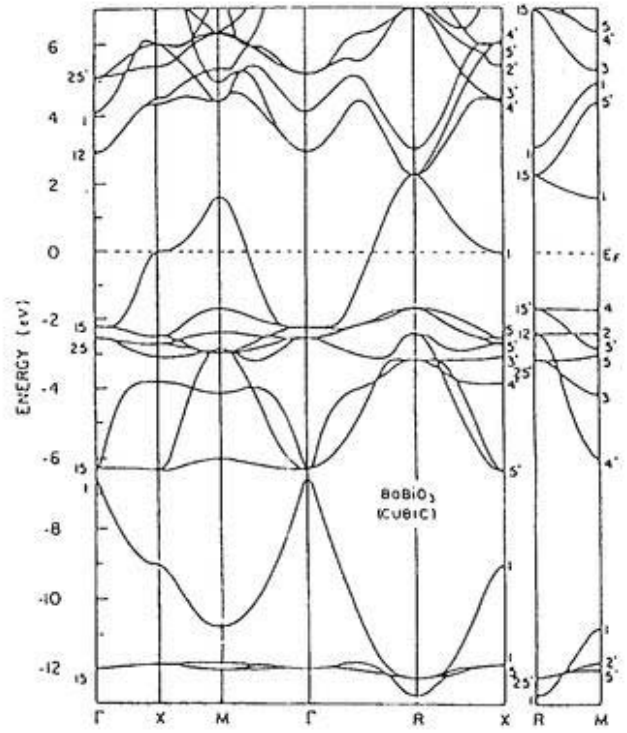

Fig. 2.6. The LAPW band structure for simple cubic $BaBiO_3$. From Ref. [4].

The $O_{2p} - Bi_{6s}$ bonding states are rather deep and located around -7 to -13 eV, whereas, the antibonding one that are mainly composed of Bi-6s orbitals, are located near the Fermi level (E_f). The electronic states of the Ba atom do not contribute to the band near the Fermi energy, and no conduction electron is found at the Ba site. According to their calculations for assuming the ideal simple cubic perovskite structure, it is found to be metallic in spite of the perfectly nested Fermi surface.

However, such a nested Fermi surface is susceptible to electronic instabilities. In the bismuthates, this leads to a Peierls distortion, in which the O

atoms surrounding every alternate Bi site are displaced towards them. This is the breathing mode displacement of the oxygen octahedra, which doubles the unit cell and thereby opens up a gap along the entire noninteracting Fermi surface, splitting the broad conduction band into two sub-bands: a filled lower band and an empty upper one. Due to this Peierls distortion, the CDW state is formed, and the metal becomes an insulator.

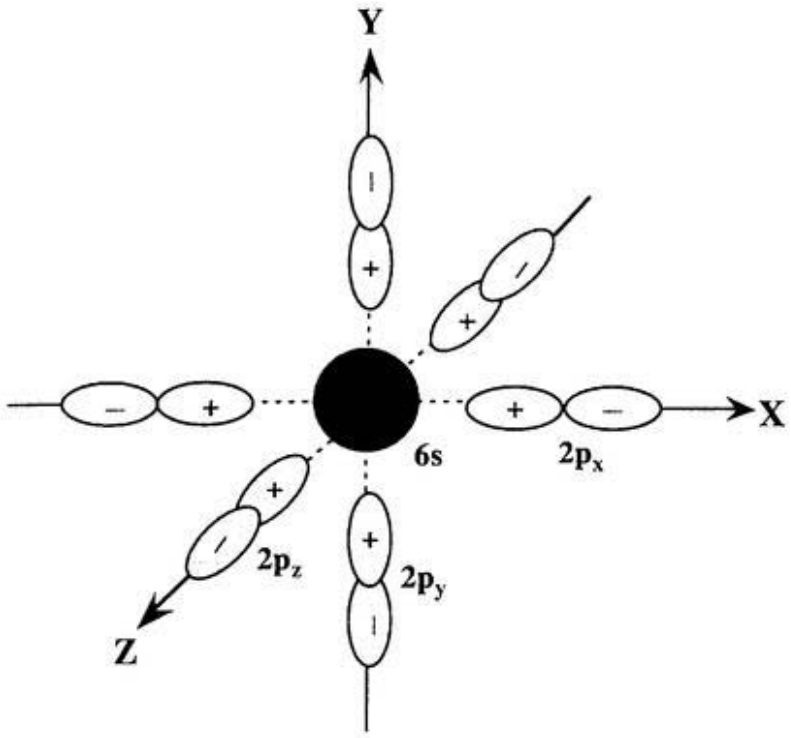

Fig. 2.7. A spherically symmetric Bi 6s orbital surrounded by the oxygen p orbitals in the BiO_6 octahedron. Only the σ orbitals of each of the six O atoms are shown.

In this CDW state, the displacement of oxygen raises and lowers the energy levels of Bi ($6s^1$) orbitals alternately along all Cartesian coordinate axes x, y and z, as schematically shown in Fig. 2.8(a).

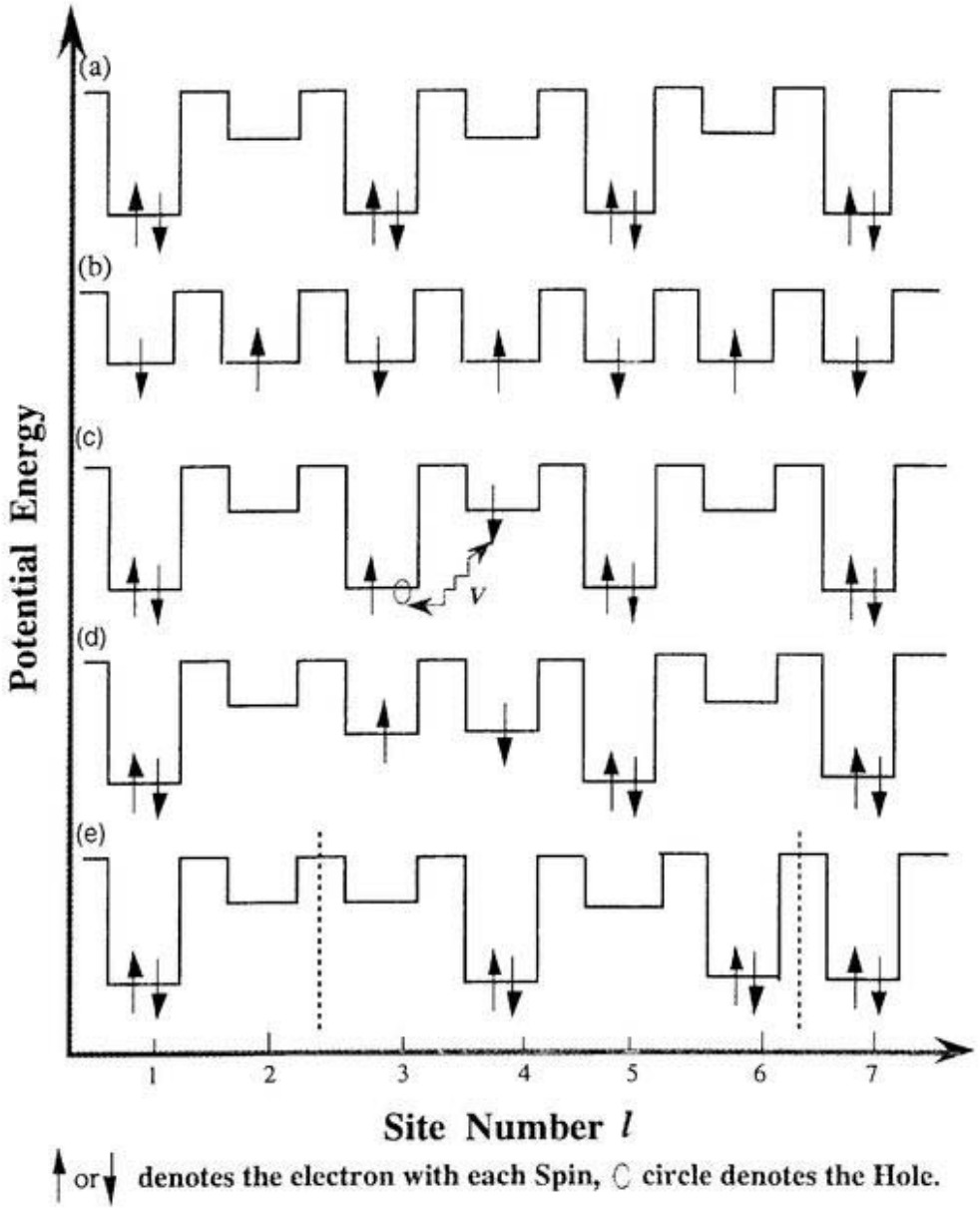

Fig. 2.8. Schematic potential energy for the 6s electron: (a) The ground state of CDW, (b) Spin density wave, (c) The charge transfer exciton, (d) The self-trapped exciton, (e) Solitons.

Liechtenstein *et al.* [21] have carried out the band structure study of $Ba_{1-x}K_xBiO_3$. For x=0, they found a lattice instability with a combination of both tilt and breathing distortions. This yields the experimentally observed

monoclinic structure. An interesting point that emerges from this band structure study is that, when details are put in, $BaBiO_3$ may have a rather small indirect band gap, which is shown in Fig. 2.9. The value of this gap, gleaned from Fig. 2.9, is roughly 0.025 Ry (≈0.34 eV). However, optical experiments must be able to see this, as a phonon assisted transition.

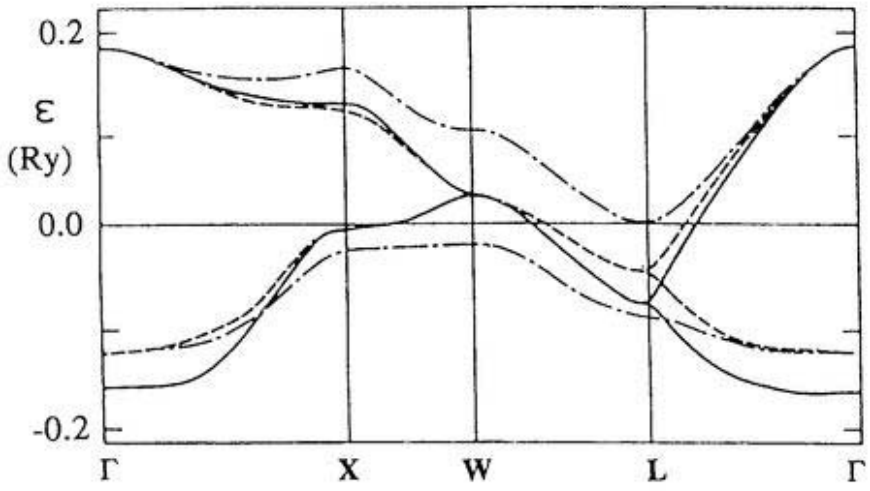

Fig. 2.9. The full potential LMTO band structure near Fermi level for $2\,BaBiO_3$. Solid line is for t=0 and b=0, dashed line is for t=10 deg and b=0. dot-dashed line is for t=10 deg and b=0.194 Å. The Brillouin zone has folded. From Ref. [21].

Therefore, our one purpose in the present work, is to reproduce the aforementioned LAPW energy band near the Fermi level by using our unified theory. By using our theory, we will finally show that, due to strong el-ph interaction, the broad conduction band near the Fermi level is split, and produces CDW state, which will be shown in Sects. 4.4 and 4.5. In our theoretical model, we will only consider the breathing mode distortion of the lattice. Tilting will not be consider, to avoid the model too complicated.

This section contains an overview of the experimental data related to the optical properties of $BaBiO_3$. During the last few years, much works have been done on the nature of the CDW insulating state as well as optical studies on BBO. The observed spectral shape of this material is quite different from a typical absorption edge of an ordinary insulator such as GaAs. The spectral shape near the visible region rather resembles the inter-band excitation across the energy gap of an ordinary insulator. While, we also have a long absorption tail extending towards the near-infrared region. Thus the overall spectrum has a good contrast to the ordinary CDW type insulator, in which a sharp light absorption peak appears only in the visible region.

In order to investigate the optical gap in BBO, Blanton *et al.* [26] have measured the reflectivity spectrum of $Ba_{1-x}K_xBiO_3$ as a function of doping x, from x=0 to x=0.4 in the frequency range from 250 to 25000 cm^{-1}. Their data on optical conductivity indicate that it has a peak at 16000 cm^{-1} in the case of CDW, as shown in Fig. 2.10. They claim that this broad peak has evolved from excitations across the single-particle (CDW) gap of BBO. Tajima *et al.* [7] also performed the resonant Raman scattering measurements, and in their experiments, a sharp absorption peak is observed near 2.0 eV, as shown in Fig. 2.11.

Raman experiments [28,29] on $BaBiO_3$ show the resonant enhancement, and appearance of higher harmonics of the 570 cm^{-1} phonon mode (breathing mode), which indicate that the optical gap is related to the strong electron phonon interaction in the system [28,30]. Inoue *et al.* [31] have reported the infrared and Raman scattering spectra of $BaBiO_3$. They have shown that the infrared activeness of the Bi-Bi stretching mode is one of the direct evidence for

the charge disproportionation between Bi sites. If neighboring two Bi's are equivalent, this stretching mode is infrared inactive but only Raman-active. In fact, the oscillator strength of this mode decreases as the doping increases, and accordingly CDW order disappears. This means that the ordered structure of CDW makes the Bi-Bi stretching mode infrared active.

Uwe *et al.* [24] have measured the light absorption spectrum of BBO at near infrared region, and they found a long absorption tail, which has a square root type shape at temperature 300 K, as shown in Fig. 2.12. They also mentioned that the prominent peaks below frequency 2000 cm^{-1} are due to overtones of LO phonon.

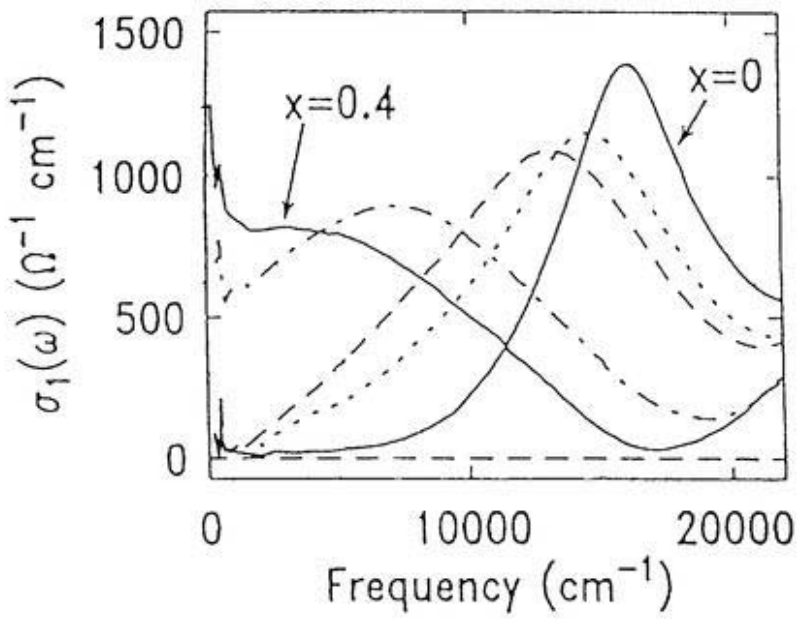

Fig. 2.10. Optical conductivities of $Ba_{1-x}K_xBiO_3$ samples, with x=0.0 (Solid line). From Ref. [26].

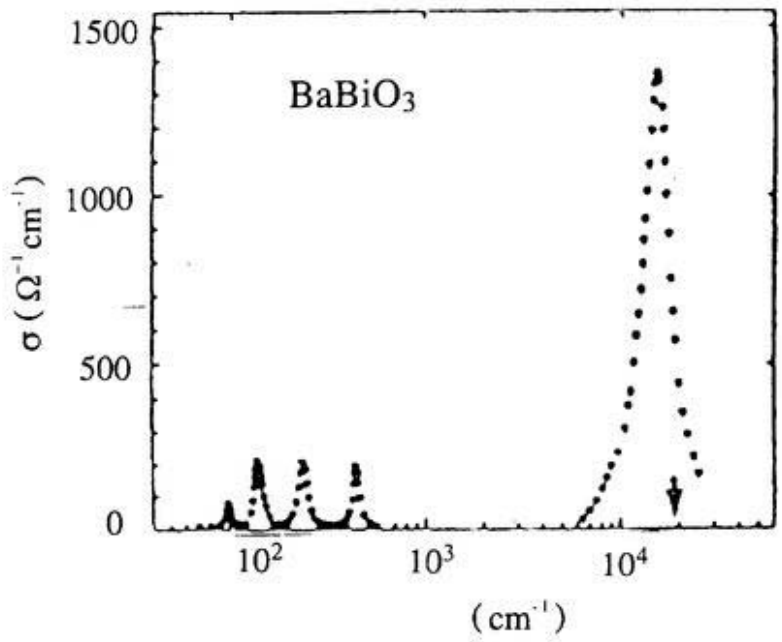

Fig. 2.11. Optical conductivity spectrum for $BaBiO_3$. From Ref. [7].

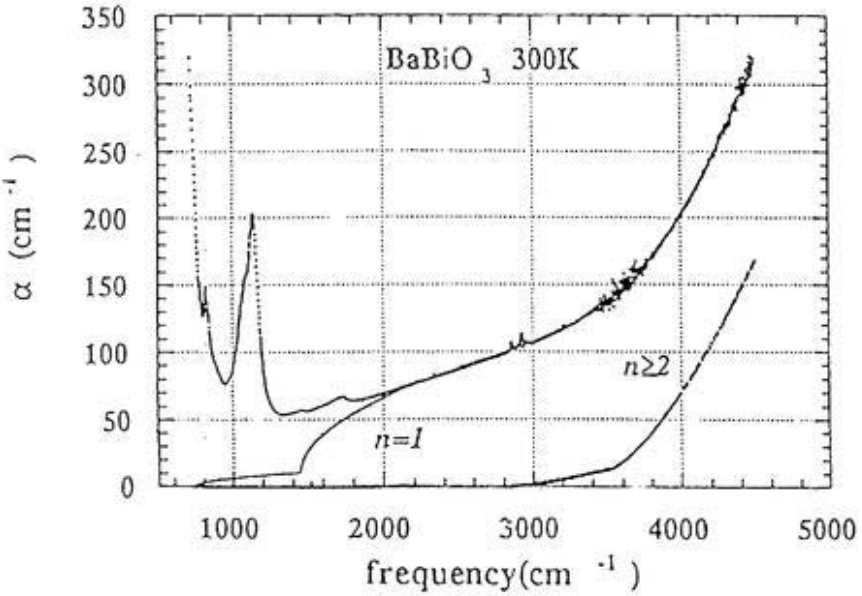

Fig. 2.12. Absorption coefficient of $BaBiO_3$. From Ref. [24].

We have already mentioned that the $BaBiO_3$ is the parent material for high-T_c superconductor $BaPb_{1-x}Bi_xO_3$ and $Ba_{1-x}K_xBiO_3$ systems. The superconducting phase occurs [2,3,45,47] in the concentration range $0.05<x<0.30$ for BPBO, and $0.37<x<0.60$ for BKBO. The highest T_c is 12 K at $x=0.25$ for the former, and 30 K at $x=0.40$ for the latter. If this latter material had been discovered two years earlier, it would be a record holder, and would cause a great sensation. The density of states at the Fermi level for both these bismuthate systems are quite low [48,49]. Although the density of states at the Fermi level is low, and also they have three dimensional structures, the superconducting transition temperatures are very high indeed. The insulating nature of BBO and the metal-insulator transition that occurs on doping with Pb or K cannot understood on the basis of band structure calculations [4,50]; they yield a half-filled conduction band for $BaBiO_3$. The simplest explanation for the insulating nature of BBO invokes a CDW instability, which opens a gap in the conduction band. Both Pb and K doping should inhibit CDW ordering for two reasons: first, such doping moves the Fermi level down from its position at half filling, and second it introduces disorder. For BBO, the top of the occupied Bi 6s band is located ~0.3 eV below E_f. Doping with K (x=0.0 to 0.3) the top of the occupied Bi 6s band moves towards E_f [51], and touches it, indicating that the system becomes metallic.

It is reasonable to compare here the properties of high-T_c cuprates with bismuthates superconductor. Strongly hybridized bands (Cu 3d O 2p for the cuprates and Bi/ Pb 6s O 2p for the bismuthates) characterize both these high T_c superconductors, in which Fermi level falls within the uppermost σ antibonding subband, making it nearly half-filled. In the cuprates this band is

formed by the σ bonding between Cu $3d(x^2 - y^2)$ and the 2p orbitals of the four surrounding oxygen atoms, and in the bismuthates, by the σ bonding between the spherically symmetric and spatially extended Bi/Pb 6s orbitals and the 2p orbitals of the six surrounding oxygen atoms. Like the bismuthates, the cuprates also have a nested Fermi surface (two dimensional as opposed the three dimensional one in the bismuthates) at zero doping. A system with a nested Fermi surface is susceptible to various instabilities like spin density wave (SDW), CDW, etc. The nominal valence of Bi in the bismuthates is 4^+ and that of Cu in the cuprates is 2^+, which means that Bi and Cu ions have just one electron in their outer shells in these compounds. Thus one should expect these oxides to show fully developed magnetic moments in their insulating states, however these two systems show very different magnetic behavior. The cuprates show a moment whereas the bismuthates are perfectly diamagnetic and there is no indication of a moment. In addition, the insulating phase of the cuprates is antiferromagnetically ordered, but in the bismuthates it exhibits CDW ordering. These differences suggest that the low energy degrees of freedom in the cuprates are the spin degrees of freedom, whereas those in the bismuthates are the charge degrees of freedom.

So we see that the bismuthates are qualitatively different from high-T_c cuprate superconductors. Their superconducting and normal state properties make these bismuthates interesting, and an attempt to understand them a challenging task. So far there has been no fully successful theoretical treatment of these systems for all ranges of doping. To understand the mechanism of superconductivity in this material more clearly, it is necessary to elucidate the electronic structure and the optical properties as well as nonlinear lattice relaxation of these materials.

3. NONLINEAR LATTICE RELAXATION OF CHARGE TRANSFER EXCITONS

The problems related with the lattice relaxation process of optical excitations in insulating solids are the subjects of considerable interest in recent years, both theoretically and experimentally.

As is well known, the exciton immediately after the light excitation is in a wave like state extending over the crystal, since the light is a plane wave. This state is usually called *Free* (F) state of exciton, and it is nothing but the Franck-Condon state. After the lattice relaxation having been completed, however, the exciton is a localized state, provided the exciton-phonon interaction is sufficiently strong, because in this state the exciton is trapped by a self-induced local lattice distortion. This state is usually called *self-trapped* state of exciton (STE), schematically shown in Fig. 2.8(d).

So, exciton created by photon in an insulator interacts with the lattice vibrations and this interaction brings about various lattice relaxation processes. In the case of an ordinary insulator, the total number of excitons is kept unchanged during this relaxation, except when excitons is created up to a very high density by intense laser light. Thus, the relaxation of low density excitons in ordinary insulators can be called a *linear lattice relaxation*. On the other hand, the CDW state is a special type of insulator that is brought about from the metallic state through the Peierls transition, and therefore, its ground state has a degeneracy or a multistability. In this multistable situation, an exciton, created by a photon from one of the ground states, proliferates during the lattice relaxation process and finally relaxes down to a collective excited state, which encompasses more than two ground states. The term *nonlinear lattice*

relaxation is introduces so as to emphasize this characteristic, in comparison with ordinary insulators.

3.1 LATTICE RELAXATION IN ONE DIMENSIONAL SYSTEM

Although the purpose of our study is three dimensional system. For the time being, let us review the aforementioned nonlinearity by taking halogen-bridged mixed-valence metal complexes (HMMC) [52] as one of the typical examples for quasi one-dimensional CDW system. In Fig. 3.1, schematically shown the relevant adiabatic energies as a function of an order parameter ($\equiv Q$), which denotes the displacement of X^- (X=Cl,Br,I) from the middle point of the adjacent two M's (M=Pt,Pd,Ni) [53]. It is nothing but the Peierls type lattice distortion. The solid line denotes the ground state, and the dashed line denotes the excited one.

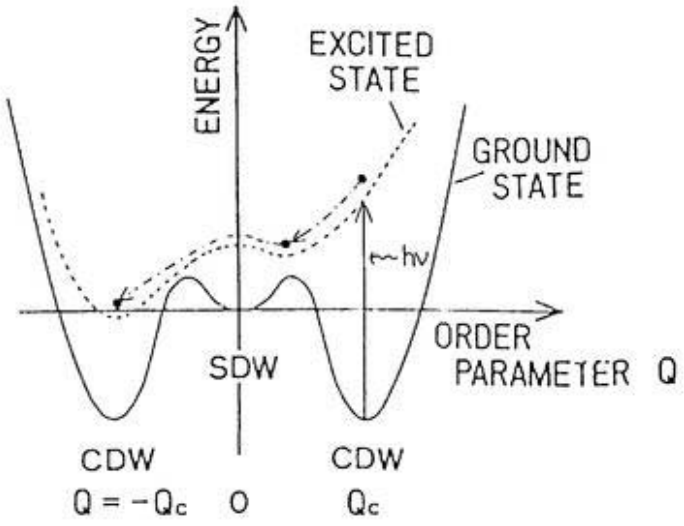

Fig. 3.1. Schematic potential energy surfaces of ground and excited states as a function of the CDW-type order parameter Q. From Ref. [53].

As shown in this figure, there are three minimum energy points in the ground state. The two minima where Q is equal to Q_c or -Q_c corresponds to the CDW states. They have different phases of the Peierls distortion of X^-. When the electron-electron coulombic repulsion is taken into account, we get another energy minimum at Q=0, in addition to these CDW states. In this configuration, the up and down spins are arranged alternately along the metallic sites M's to make this repulsion weak, as shown in Fig. 2.8(b). This is the SDW, and the relative stability between this state and the aforementioned CDW one is determined by the competition between the el-ph interaction and the coulombic repulsion [54].

Referring to Figs. 2.8 and 3.1, let us briefly see the nonlinear lattice relaxation process of the exciton. The HMMC has a strong light absorption band in the visible region [55], which corresponds to the charge transfer (CT) excitation of an electron from the occupied d_{z^2} orbital to the vacant ones, as shown in Fig. 2.8(c). Thus an electron and a hole are created, and they attract each other through the inter-orbital coulombic force. Such a state is called a CT exciton. In Fig. 3.1, this type of photoexcitation from one of the CDW ground states is represented by a vertical arrow. Once the exciton has been created, it will relax down through the potential curve of the excited state, and induces a local lattice distortion around it.

This photoexcitation is nothing but a backward charge transfer, and the electron number per orbital becomes almost equal in this local region (Fig. 2.8(c)) and, therefore, the Peierls distortion has lost the reason for its presence. Hence, it tends to disappear, as seen from Fig. 2.8(d). Thus the exciton self-induces a local lattice distortion and is trapped in it, by producing STE. However, since this STE appears near the point with Q=0, the SDW type spin order is also expected to appear in this localized state.

As seen from Fig. 3.1, the STE is expected to undergo further relaxations. In the CDW, as is well known, we have a low-lying excited state with a collective nature. That is one phase of the ground state can appear locally in the other phase of the ground state, at the expense of creating boundaries between two phases. This boundary is usually called a soliton, and the exciton is expected to relax finally down to the state with a pair of solitons, as shown in Fig. 2.8(e). Experimentally this type of low-lying excited states was observed in the photoinduced measurements [56-58].

3.2 LATTICE RELAXATION IN THREE DIMENSIONAL SYSTEM

Keeping these one dimensional results in mind, let us return back to the three dimensional case. So, in this section, we will be concerned with the nonlinear lattice relaxation of exciton in $BaBiO_3$, as a typical example of three-dimensional CDW state. Much of theoretical, as well as experimental works have been done on one and two-dimensional CDW system in connection with lattice relaxation. However, very few experimental works are performed on three dimensional system like $BaBiO_3$, and in the present, there is no systematic theoretical study to explain the experimental work related to relaxation in this material.

In $BaBiO_3$ there are two type of gaps exist i.e. direct and indirect gaps, and the appearance of this direct and indirect gaps are due to the characteristic and complicated nature of the one electron energy band $E(k)$ around the Fermi level. Its depends on the nature of three dimensional chemical bonds among the s-orbital of the metallic atoms and the three p-orbitals of O's atom. As a result, it often occurs that even after the CDW type metal-insulator transition, optical excitations appear below the CDW gap. In this case, we have a mid-gap

absorption, which is not due to the collective excitations in the gap such as solitons, as described in the previous section, but simply due to the complicated k-dependency of the one electron energy band. Recently, this type of low energy optical excitation is found below the CDW gap of BBO [33-37]. Federici *et al.* [35] indicates the possibility of indirect photoexcitation of the polaron via direct relaxation. Their schematic explanation is shown in Fig. 3.2. However, its physical reason is not so clear. Taliani *et al.* [37] measured the photoinduced absorption of $BaBiO_3$. Their result is shown in Fig. 3.3.

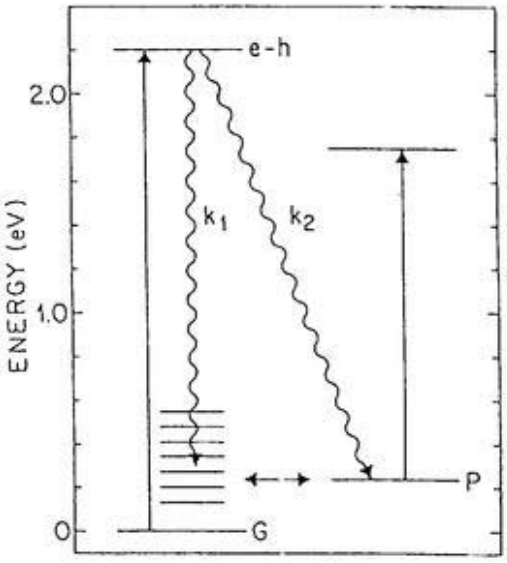

Fig. 3.2. Schematic energy level diagram and relaxation path-ways for $BaBiO_3$. The labels G, e-h, and P represent the ground state, the photogenerated electron and hole, and polaron, respectively. From Ref. [35].

Photoinduced reflectance measurements [33] of $BaBiO_3$ are reported and several new peaks in the reflectance spectra are observed around the mid gap energy, as shown in Fig. 3.4. All of these results indicate the evidence for the lattice relaxation after removing electrons from the valence band, and as a consequence energy levels appear within the gap, resulting in mid gap states.

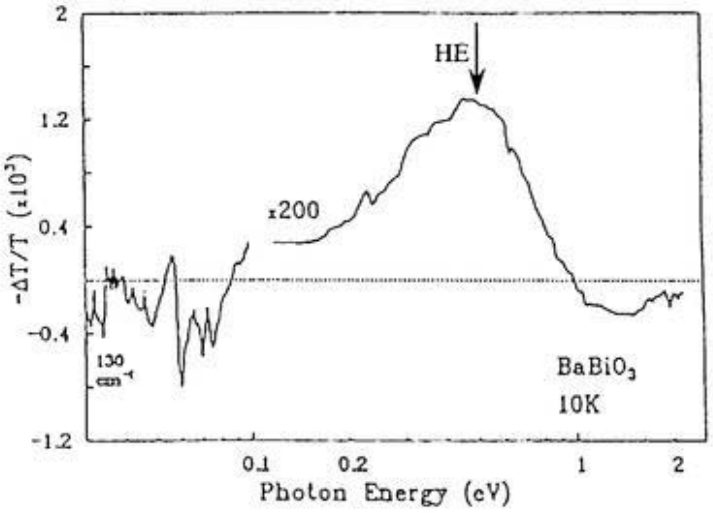

Fig. 3.3. Photoinduced infrared absorption (left side) and photomodulation (2000 Hz) absorption (right side) of $BaBiO_3$ at 10K. From Ref. [37].

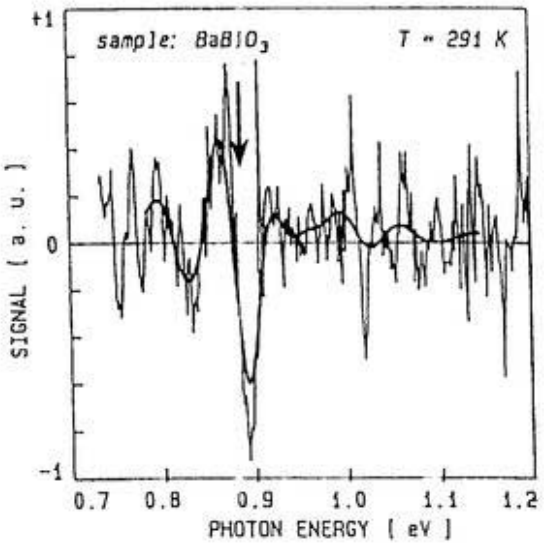

Fig 3.4. Photoinduced reflectance spectrum of a $BaBiO_3$ sample. Thin line: as measured; thick line: smoothed. From Ref. [33].

In chapter 6, we will present our theoretical result to clarify this lattice relaxation process, and the origin of this photoinduced absorption.

4. THEORY AND MODEL FOR $BaBiO_3$

4.1 MODEL HAMILTONIAN

To describe the aforementioned direct and indirect excitations as well as their nonlinear lattice relaxations in $BaBiO_3$, let us now introduce the following extended Peierls-Hubbard model in a cubic lattice ($\hbar$=1):

$$H = \sum_{\langle\langle l,l'\rangle\rangle}\sum_{\sigma} T_{ll'}(a^{\dagger}_{l\sigma}a_{l'\sigma} + h.c.) + U\sum_{l} n_{l\alpha}n_{l\beta} + V\sum_{\langle l,l'\rangle}\sum_{\sigma,\sigma'} n_{l\sigma}n_{l'\sigma'}$$

$$+\sqrt{S\omega_0}\sum_{l,\sigma} Q_l n_{l\sigma} + \omega_0\sum_{l}\left(\frac{Q_l^2}{2} - \frac{1}{2}\frac{\partial^2}{\partial Q_l^2}\right),\ n_{l\sigma} \equiv a^{\dagger}_{l\sigma}a_{l\sigma}. \qquad (4.1.1)$$

Here, $a^{\dagger}_{l\sigma}(a_{l\sigma})$ creation (annihilation) operator of an electron at a lattice sites $l(\equiv l_x, l_y, l_z)$ with spin $\sigma(\equiv \alpha, \beta)$. $T_{ll'}$ is the transfer energy of an electron between two lattice sites l and l'. The unit of length is the lattice constant. To describe the energy band of the metallic state of BBO in detail, we have taken into account four types of transfer energies between various neighbouring lattice sites, named T_1, T_2, T_3 and T_4, as shown in Fig. 4.1. It should be noted that the real Wannier function corresponding to $a^{\dagger}_{l\sigma}$ is a linear combination of the Bi(6s) and the O(2p) orbitals. It is centered at a certain lattice site of Bi atom in a perovskite type structure, but is extended widely to various other sites, due to the extended nature of s-orbitals. In this situation, the $T_{ll'}$ is not limited only within the first nearest neighbor. That is the reason why we have to use these four types of transfer energies.

The parameters U and V in eq. (4.1.1) denote the intra-site and inter-site Coulomb energies, respectively. Here $\langle\langle l,l'\rangle\rangle$ means an arbitrary pair of Bi sites,

while $\langle l, l' \rangle$ means nearest neighbour one. The fourth term of eq. (4.1.1) denotes the electron-phonon (el-ph) coupling and S is its coupling constant. Q_l is the site-localized phonon mode with frequency ω_0, and corresponds to the breathing motion of six O atoms around Bi, as schematically shown in Fig. 2.3. The fifth term is the energy of this phonon mode. Since the phonon energy is expected to be sufficiently small, $\omega_0 << (T_1, U, V, S)$, we can use the adiabatic approximation $(\omega_0 \to 0)$, neglecting the kinetic energy term of the phonon in eq. (4.1.1). In this case, the phonon can be treated as a classical distortion of the lattice.

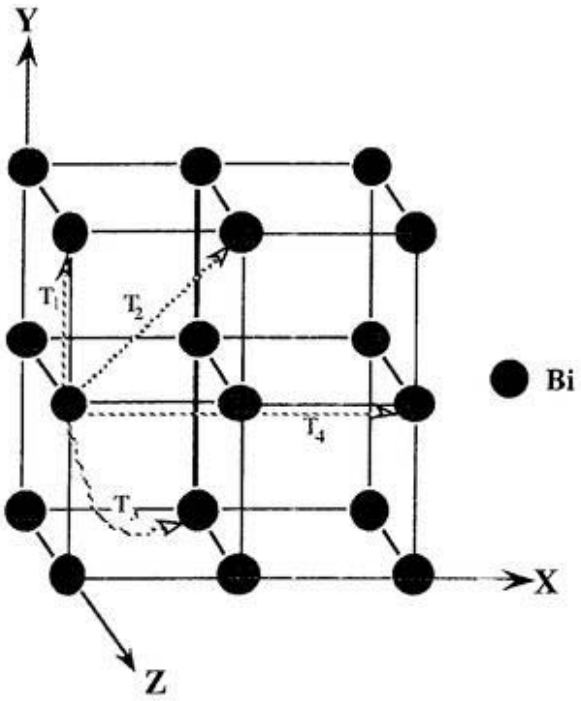

Fig. 4.1. Four types of transfer energies T_1, T_2, T_3 and T_4.

Introducing $h(\equiv H/T_1)$, $t_{ll'}(\equiv T_{ll'}/T_1)$, $u(\equiv U/T_1)$, $v(\equiv V/T_1)$, $s(\equiv S/T_1)$ and $q_l(\equiv \sqrt{\omega_0/S}Q_l)$, we rewrite eq. (4.1.1) into a dimensionless form as

$$h = -\sum_{\langle\langle l,l'\rangle\rangle}\sum_{\sigma} \mathrm{t}_{ll'}(a^{\dagger}_{l\sigma}a_{l'\sigma} + h.c.) + \mathrm{u}\sum_{l} n_{l\alpha}n_{l\beta} + \mathrm{v}\sum_{\langle l,l'\rangle\sigma,\sigma'}\sum n_{l\sigma}n_{l'\sigma'}$$

$$+\mathrm{s}\sum_{l,\sigma} q_l n_{l\sigma} + \mathrm{s}\sum_{l} q_l^2 / 2. \qquad (4.1.2)$$

In order to determine its ground state, we can now use the Hartree-Fock (HF) approximation for the inter-electron coulombic interactions. In this case, it is expedient to divide h formally into the HF Hamiltonian ($\equiv h^{HF}$) and the fluctuations ($\equiv \Delta h_c$ and $\equiv \Delta h_p$) therefrom, due to the electron-electron and electron-phonon interactions as

$$h = h^{HF} + \Delta h_c + \Delta h_p. \qquad (4.1.3)$$

In this Hartree-Fock approximation, we have decoupled the coulombic repulsion's between two electrons, and hence h^{HF} is given by

$$h^{HF} = -\sum_{\langle\langle l,l'\rangle\rangle}\sum_{\sigma}\{(\mathrm{t}_{ll'} + \mathrm{v}\langle m_{ll'\sigma}\rangle)a^{\dagger}_{l\sigma}a_{l'\sigma} + h.c.\}$$

$$+\mathrm{u}\sum_{l,\sigma}(\langle n_{l,-\sigma}\rangle n_{l\sigma} - \langle n_{l\sigma}\rangle\langle n_{l,-\sigma}\rangle / 2)$$

$$+\mathrm{v}\sum_{\langle l,l'\rangle\sigma,\sigma'}\sum(\langle n_{l\sigma}\rangle n_{l'\sigma'} + \langle n_{l'\sigma'}\rangle n_{l\sigma} - \langle n_{l\sigma}\rangle\langle n_{l'\sigma'}\rangle) + \mathrm{v}\sum_{\langle l,l'\rangle}\sum_{\sigma}\left|\langle m_{ll'\sigma}\rangle\right|^2$$

$$+\mathrm{s}\sum_{l,\sigma}\bar{q}_l n_{l\sigma} + \mathrm{s}\sum_{l}\bar{q}_l{}^2 / 2. \qquad (4.1.4)$$

Here, $m_{ll'\sigma}$ is defined as $m_{ll'\sigma} \equiv a^{\dagger}_{l\sigma}a_{l'\sigma}$, and the angle brackets $\langle\cdots\rangle$ appeared above, denote the average of $\cdots$ with respect to this HF ground state ($\equiv |g\rangle$)

$$\langle \cdots \rangle \equiv \langle g | \cdots | g \rangle . \tag{4.1.5}$$

While, $\bar{q}_l$ denotes a static lattice distortion. At present, however, this ground state is not known yet, but will be determined self-consistently afterwards. The fluctuations terms of eq. (4.1.3) are given as

$$\Delta h_c = \mathrm{u} \sum_l \Delta n_{l\alpha} \Delta n_{l\beta} + \mathrm{v} \sum_{\langle l,l' \rangle} \sum_{\sigma,\sigma'} \Delta n_{l\sigma} \Delta n_{l'\sigma'}$$

$$+\mathrm{v} \sum_{\langle l,l' \rangle} \sum_{\sigma} (\langle m_{ll'\sigma} \rangle m_{l'l\sigma} + \langle m_{l'l\sigma} \rangle m_{ll'\sigma} - \langle m_{ll'\sigma} \rangle \langle m_{l'l\sigma} \rangle), \tag{4.1.6}$$

$$\Delta h_p = \mathrm{s} \sum_{l,\sigma} \Delta q_l \Delta n_{l\sigma} + \mathrm{s} \sum_l \Delta q_l (\langle n_{l\alpha} \rangle + \langle n_{l\beta} \rangle + \bar{q}_l) + \mathrm{s} \sum_l \Delta q_l{}^2 / 2, \tag{4.1.7}$$

$$n_{l\sigma} \equiv \langle n_{l\sigma} \rangle + \Delta n_{l\sigma} , \tag{4.1.8}$$

$$q_l \equiv \bar{q}_l + \Delta q_l . \tag{4.1.9}$$

Here, $\langle n_{l\sigma} \rangle$, $\bar{q}_l$ and $\langle m_{ll'\sigma} \rangle$ are also unknown parameters, and should be determined self-consistently.

4.2 GROUND STATE OF THE CDW

The CDW instability originates from the frozen breathing type displacement of oxygen around Bi atoms. In this state, O atoms displaces alternately in the opposite direction along the all Cartesian axes (x, y and z), as shown in Fig. 2.3(a), and leads to the charge disproportionation of $Bi^{3+}$and Bi^{5+} between two neighbouring Bi sites. As a result, the energy levels of Bi 6s orbitals raise and

lower alternately, and two electrons with opposite spins occupy the lower energy sites, as shown in Fig. 2.6(a). Thus the displacement of oxygen $\bar{q}_l$, can be described as

$$\bar{q}_l = (-1)^l q - 1, \tag{4.2.1}$$

where $(-1)^l q$ denote the Peierls distortion in the ground state of the CDW, and q is its amplitude. This q should be determined beforehand, within the mean-field theory, while -1 denote the uniform displacement. As $\langle n_{l\alpha} \rangle$ is equal to $\langle n_{l\beta} \rangle$ in the CDW ground state, the average $n_{l\sigma}$ is given by

$$\langle n_{l\sigma} \rangle = (-1)^l \delta n_\sigma + 1/2. \tag{4.2.2}$$

Here δn_σ is the deviation from 1/2 for the number of electron with σ spin. We also assumed that the bond density $m_{l'l\sigma}$ is independent of the site l, and so it becomes a constant

$$\langle m_{ll'\sigma} \rangle = \langle m_{l'l\sigma} \rangle = \bar{m}. \tag{4.2.3}$$

As $\bar{q}_l$ is given by eq. (4.2.1), we can now calculate the energy of the CDW ground state of this three dimensional BBO system with N-sites and N-electrons from eq. (4.1.4). Inserting eqs. (4.2.1)-(4.2.3) into eq. (4.1.4), we get as

$$h^{HF} = -\sum_{\langle\langle l,l' \rangle\rangle} \sum_{\sigma} \{(\mathrm{t}_{ll'} + \mathrm{v}\bar{m}) a^{\dagger}_{l\sigma} a_{l'\sigma} + h.c.\} + \sum_{l\sigma} (-1)^l \{\mathrm{u}\delta n_{-\sigma} - 6\mathrm{v}\delta n_{+}$$

$$+\mathrm{s}q\} n_{l\sigma} + N\{\mathrm{s}q^2/2 + \mathrm{v}(\delta n_{+})^2 - \mathrm{u}\delta n_\alpha \delta n_\beta + 2\mathrm{v}\bar{m}^2\}$$

$$+N(-\mathrm{s}/2 + \mathrm{u}/4 + \mathrm{v}). \tag{4.2.4}$$

Here $\delta n_+ = \delta n_\alpha + \delta n_\beta$. We should note again that, in the case of CDW, the charge density waves of electron with opposite spins occur only in phase, i.e.

$$\delta n \equiv \delta n_\alpha = \delta n_\beta. \tag{4.2.5}$$

As is well known, the adiabatic approximation is to minimize the electronic energy with respect to electronic variable δn_σ and $\overline{m}$ for a given lattice configuration q, and after that, the total energy is to be minimize with respect to q. Therefore, the amplitude of the Peierls distortion q can be obtained from the Feynman-Hellman's theorem:

$$\frac{\partial \langle h^{HF} \rangle}{\partial q} = 0. \tag{4.2.6}$$

Thus, we get a balance equation between the distortion and the charge density as

$$q = -\delta n_+, \tag{4.2.7}$$

and substituting it into eq. (4.2.4), we can eliminate q. So, we can now determine the ground state $|g\rangle$ and its energy, by using the self-consistently calculated parameters, δn_σ and $\overline{m}$.

To determine the one-body eigenvalues and eigenfunctions of h^{HF} practically, let us rewrite the eq. (4.2.4) as the following

$$h^{HF} = \sum_\sigma \mathrm{a}_\sigma^\dagger M_\sigma \mathrm{a}_\sigma + const., \tag{4.2.8}$$

$$\begin{aligned} const. = N\{\mathrm{s}q^2/2 + \mathrm{v}(\delta n_+)^2 - \mathrm{u}\delta n_\alpha \delta n_\beta + 2\mathrm{v}\overline{m}^2\} \\ +N(-\mathrm{s}/2 + \mathrm{u}/4 + \mathrm{v}), \end{aligned} \tag{4.2.9}$$

where $\mathrm{a}_\sigma^\dagger$ is the N dimensional row vector operator defined as

$$\mathrm{a}_\sigma^\dagger = (a_{1\sigma}^\dagger, a_{2\sigma}^\dagger, \cdots\cdots, a_{N\sigma}^\dagger). \tag{4.2.10}$$

M_σ is the $N \times N$ energy matrix and we do not write down these elements explicitly, since it is simple but too lengthy. From the eigen-value equation

$$M_\sigma \mathrm{f}_{\lambda\sigma} = e_{\lambda\sigma} \mathrm{f}_{\lambda\sigma}, \qquad (\lambda = 1, 2, \cdots, N), \tag{4.2.11}$$

we can get the eigenvalue ($\equiv e_{\lambda\sigma}$) and the eigenvector ($\equiv \mathrm{f}_{\lambda\sigma}$) of M_σ. Here λ is the index of eigenvector, numbered according to its energy. $\mathrm{f}_{\lambda\sigma}^\dagger$ is the N dimensional row vector:

$$\mathrm{f}_{\lambda\sigma}^\dagger = (f_{\lambda\sigma}^*(1), f_{\lambda\sigma}^*(2), \cdots\cdots, f_{\lambda\sigma}^*(N)), \tag{4.2.12}$$

where the component $f_{\lambda\sigma}^*(l)$ $(l = 1, 2, \cdots, N)$ denotes its amplitude at the site l. We, at first, numerically determine the following new operator:

$$b_{\lambda\sigma}^\dagger = \sum_l f_{\lambda\sigma}(l) a_{l\sigma}^\dagger, \tag{4.2.13}$$

that can diagonalize h^{HF} as

$$h^{HF} = \sum_{\lambda,\sigma} e_{\lambda\sigma} b_{\lambda\sigma}^\dagger b_{\lambda\sigma} + const. \tag{4.2.14}$$

So, the λth eigenvalue $e_{\lambda\sigma}$ of h^{HF}, and its eigenfunction $f_{\lambda\sigma}(l)$ is determined. λ is numbered according to their energies from lower ones to upper ones.

By using this eigenfunction, the ground state is determined as

$$|g\rangle = \prod_{\lambda}^{occ.} b^{\dagger}_{\lambda\alpha} b^{\dagger}_{\lambda\beta} |0\rangle, \quad (|0\rangle \text{ is the true electron vacuum}). \tag{4.2.15}$$

Thus we can determine the ground state $|g\rangle$ and its energy ($\equiv E_g$) by using the self-consistent parameters δn_σ and $\overline{m}$ within the Hartree-Fock approximation.

4.3 EXCITED STATES AND EXCITON

We can now roughly estimate the energies of the excited states, E'_n, within the Hartree-Fock approximation. However, we will calculate here, the excited states and its energies including the residual interactions which are neglected in the HF approximation. We will take this residual interaction into account within the subspace of one-electron excitation. These excited states are such ones that an electron is removed from an occupied level and is put into an unoccupied one. In this way, an excited electron and a hole are created, and they will bound each other through the inter-orbital coulombic force. Such a state is usually called a charge transfer (CT) exciton, which is schematically shown in Fig. 2.8(c). In order to perform this calculation, at first, we denote the excited states within the HF approximation by $|n\rangle$, which are numbered according to their energies from lower ones to upper ones, $n = 1, 2, 3, \cdots$. In the next, we have to calculate the following energy matrix elements,

$$E'_{nn'} = \langle n | h^{HF} | n' \rangle. \tag{4.3.1}$$

Since h^{HF} has already been diagonalized, we can simply rewrite eq. (4.3.1) as

$$E'_{nn'} = \delta_{nn'} \langle n | h^{HF} | n \rangle. \tag{4.3.2}$$

We also have to evaluate the energy matrix element coming from Δh_c in eq. (4.1.6). It is given as

$$\Delta E'_{nn'} = \langle n | \Delta h_c | n' \rangle. \tag{4.3.3}$$

It should be noted that this is nothing but the electron-hole attraction within the first order perturbation theory for Δh_c, but it surely results in the exciton effect. Adding this correction term to the original HF energy matrix $E'_{nn'}$, we obtain the following total energy matrix $E_{nn'}$ as

$$E_{nn'} = E'_{nn'} + \Delta E'_{nn'}. \tag{4.3.4}$$

Since this includes off-diagonal elements, we should diagonalize it, and can obtain new eigenvalues ($\equiv E''_n$) and their eigenfunctions ($\equiv |n\rangle''$).

If we return back to eq. (4.1.3), we also have another fluctuation Δh_p. However, as for this Δh_p, we will take it into account only when we consider the effect of lattice fluctuation, and it will be explained later in details.

4.4 METALLIC STATE

In this section, we will calculate the electronic energy bands of the metallic state of $BaBiO_3$. As we mentioned before, Mattheiss and Hamann [4] have calculated the energy bands for a simple cubic BBO by using the self-consistent linear augmented plane wave method. Therefore, we will reproduce their result by using aforementioned extended Peierls-Hubbard model. For this purpose, we

neglect the intra-site el-el, and el-ph interactions, and retain the inter-site el-el interaction v in eq. (4.1.4). Introducing the following Fourier transformation with a wave vector k as

$$a_{k\sigma} \equiv \sum_{l} N^{-1/2} e^{-ik.l} a_{l\sigma}, \tag{4.4.1}$$

we get the following Hamiltonian ($\equiv h_{met.}^{HF}$) for the metallic state as

$$h_{met.}^{HF} = \sum_{k} \sum_{\sigma} E_{k}^{met.} a_{k\sigma}^{\dagger} a_{k\sigma} + \text{constant terms}, \tag{4.4.2}$$

where,

$$E_{k}^{met.} = \sum_{\ell} (t_{ll'} + v\overline{m}) e^{-ik.\ell}, \quad \ell \equiv (l - l'). \tag{4.4.3}$$

Regarding $t_{ll'}$($\equiv(T_1, T_2, T_3, T_4)$) and v as a set of adjustable parameters, we can reproduce the aforementioned band calculation. By trial and error method, assuming the T_1 is most dominant, v is sub-dominant, and others are rather small, we can finally find a set of following parameter values; T_1=0.365 eV, T_2=0.0543 eV, T_3=-0.0118 eV, T_4=-0.1205 eV and v=0.22, which gives the best fitting. There is no so much ambiguity. The resultant energy band and the density of states of this metallic state are shown in Figs. 4.2 and 4.3, respectively. It well reproduces the Mattheiss and Hamann's result as far as the aforementioned broad conduction band is concerned.

4.5 CALCULATED RESULTS OF CDW STATE

Although the metallic state is predicted from the aforemention band calculation, $BaBiO_3$, in fact, is an insulator. In view of this insulating

characteristic of BBO, we can assume that the metallic state is unstable against a perturbation of wave vector $\Omega(\equiv(\pi,\pi,\pi))$ with twice the period of the lattice,

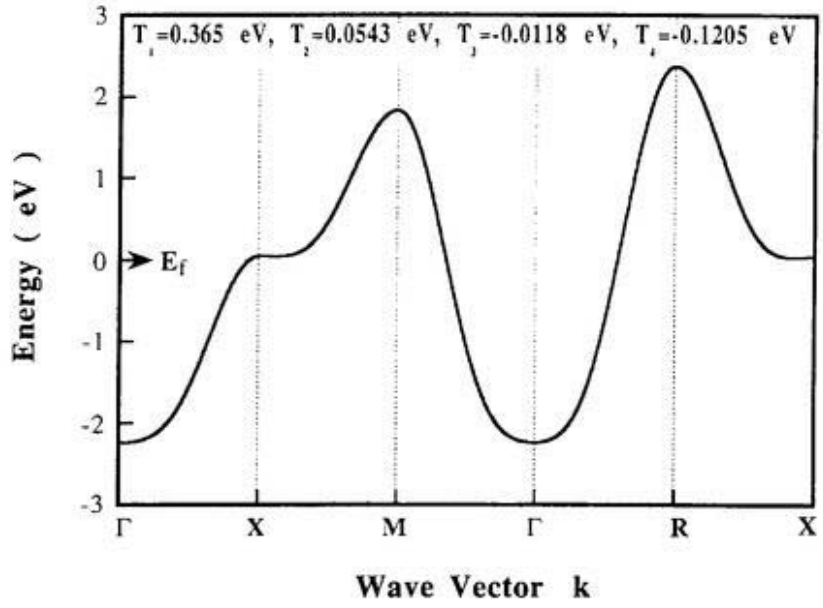

Fig. 4.2. The band dispersion of the metallic state.

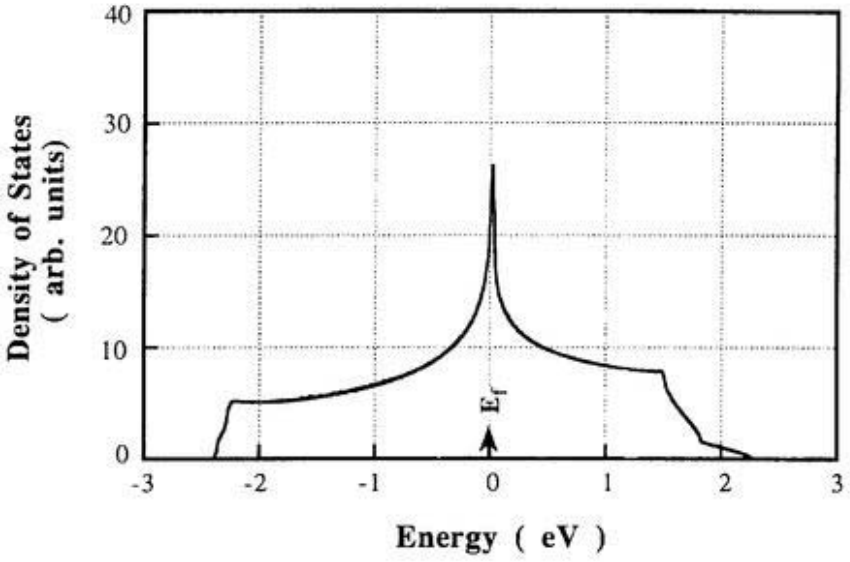

Fig. 4.3. The density of states of the metallic state.

and it opens a gap at the Fermi level, splitting the broad conduction band into two sub-bands: a filled lower band and an empty upper one. In our case, this perturbation is taken into account by the electron density wave and the lattice distortion wave through the el-el and el-ph interactions. To describe this instability, we use eq. (4.2.1), eq. (4.2.2) and eq. (4.2.3). Neglecting the two kinds of fluctuations Δh_c and Δh_p, we can rewrite the HF Hamiltonian ($\equiv h_{ins.}^{HF}$) for this insulating state as

$$h_{ins.}^{HF} = -\sum_{\langle\langle l,l'\rangle\rangle}\sum_{\sigma}\{(\mathrm{t}_{ll'} + \mathrm{v}\overline{m})a_{l\sigma}^{\dagger}a_{l'\sigma} + h.c.\} + \sum_{l,\sigma}(-1)^{l}D_{\sigma}n_{l\sigma} + c_1, \qquad (4.5.1)$$

where,

$$D_{\sigma} = \mathrm{u}\delta n_{-\sigma} - 6\mathrm{v}\delta n_{+} + \mathrm{s}q, \qquad (4.5.2)$$

and

$$c_1 = N\{\mathrm{s}q^2/2 + \mathrm{v}(\delta n_{+})^2 - \mathrm{u}\delta n_{\alpha}\delta n_{\beta} + 2\mathrm{v}\overline{m}^2\} + N(-\mathrm{s}/2 + \mathrm{u}/4 + \mathrm{v}). \qquad (4.5.3)$$

By applying Fourier Transformation, we get,

$$h_{ins.}^{HF} = -\sum_{k}\sum_{\sigma}[a_{k\sigma}^{\dagger}, a_{k+\Omega,\sigma}^{\dagger}]\begin{bmatrix} E_k^{ins.} & D_{\sigma} \\ D_{\sigma} & E_{k+\Omega}^{ins.} \end{bmatrix}\begin{bmatrix} a_{k\sigma} \\ a_{k+\Omega,\sigma} \end{bmatrix} + c_1, \qquad (4.5.4)$$

where, summation over k should be limited within the half of the first Brillouin zone, and

$$E_k^{ins.} = \sum_{\ell}(t_{ll'} + \mathrm{v}\overline{m})e^{-ik.\ell}. \qquad (4.5.5)$$

The unknown parameters q, δn_{σ} and $\overline{m}$ are determined self-consistently, as we mentioned in sub-section 4.1. By diagonalize this (2×2) matrix, we can obtain the ground state and its energy. The one-electron energy band is now splits into

lower and upper bands, and the gap appears in between. In order to describe the CDW state, we have set s=0.43 and u=1.0, so that our theory can reproduce the direct gap (E_d) and indirect gap (E_i) around 2.0 eV and 0.55 eV, respectively. The calculated energy bands and the density of states are shown in Figs. 4.4 and 4.5 respectively.

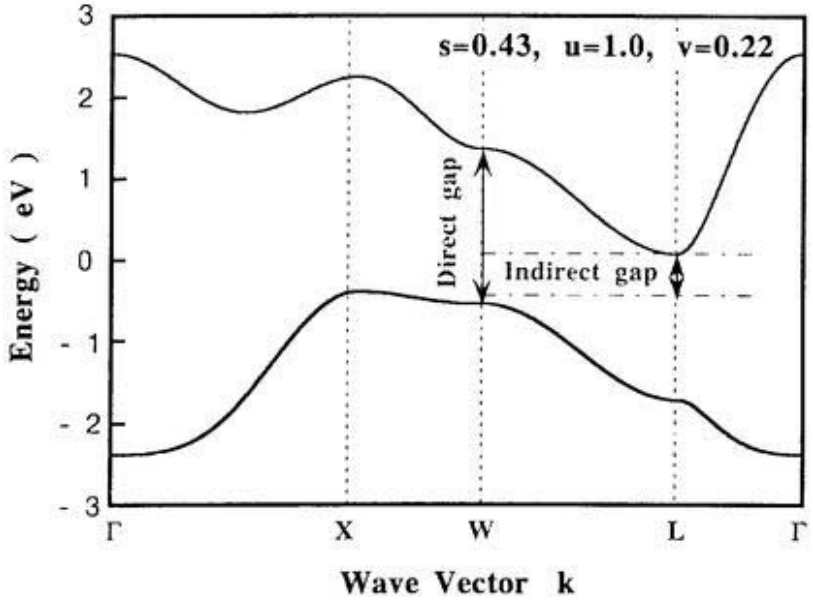

Fig. 4.4. The band dispersion of CDW state.

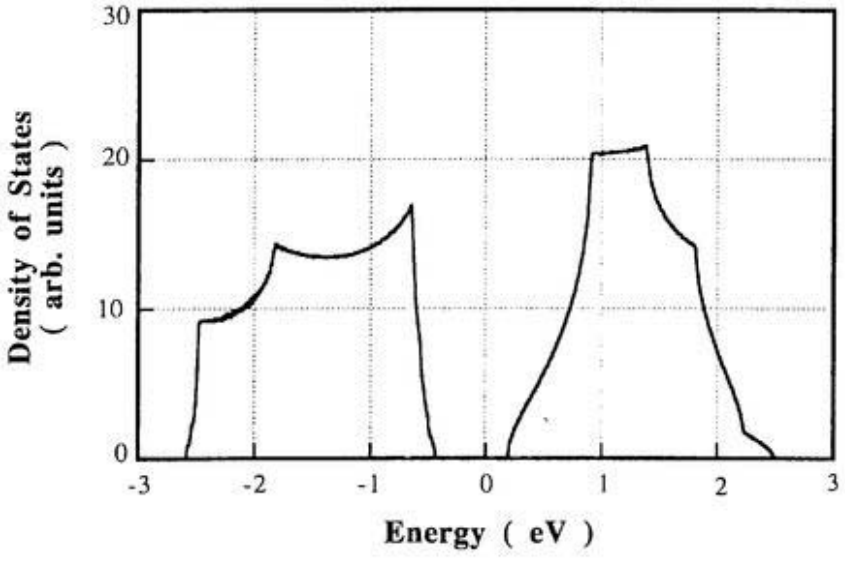

Fig. 4.5. The density of states of the CDW state.

In Fig. 4.6 the charge density distribution of the CDW state is also shown.

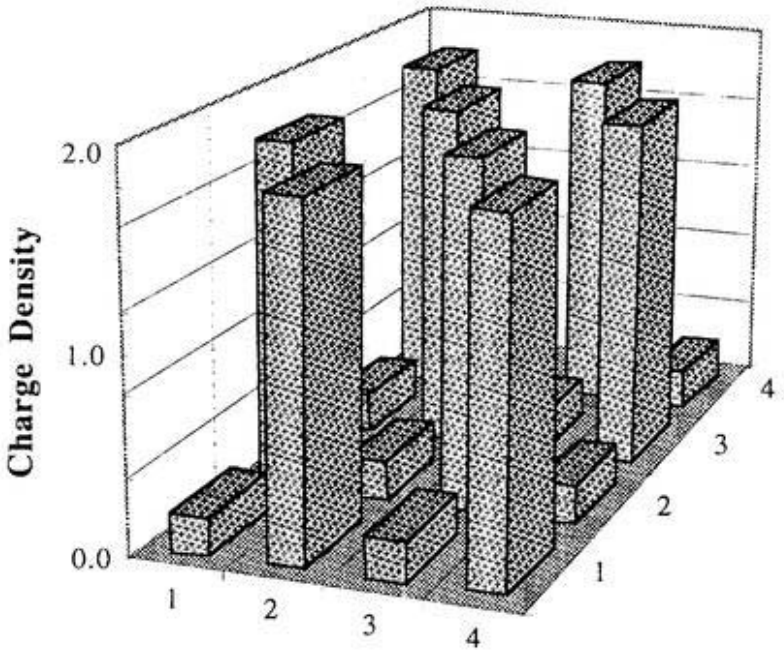

Fig. 4.6. The charge density of the CDW state on a 4×4 plane.

4.6 EXCITON BANDS

Let us now proceeds to the exciton effects, using these new one-electron energy bands thus obtained. Diagonalizing the energy matrix $E_{nn'}$ given by eq. (4.3.4), we can calculate the exciton energy bands, a part of which is shown in Fig. 4.7. It is the dispersion relation from $(0,\pi/2,0)$ to $(-\pi/2,\pi/2,\pi/2)$, along the line $(-k,\pi/2,k)$; $0 \le k \le \pi/2$. The minimum at around $(-\pi/2,\pi/2,\pi/2)$ in Fig. 4.7 mainly comes from the electron at the point L and the hole at around point X of Fig. 4.4. We can see that several kinds of exciton bands appear. In our model, the hole can exert its appreciable attraction only when the electrons is in its six nearest neighbour sites. Therefore, we can obtain six exciton bands at most. However, the total number of exciton bands which appear below the

free el-hole pair continuum is determine by the strength of inter-site coulombic repulsion v itself. In the case of Fig. 4.7, we can see only three types of exciton bands; s-type, longitudinal p-type and two transverse p-types.

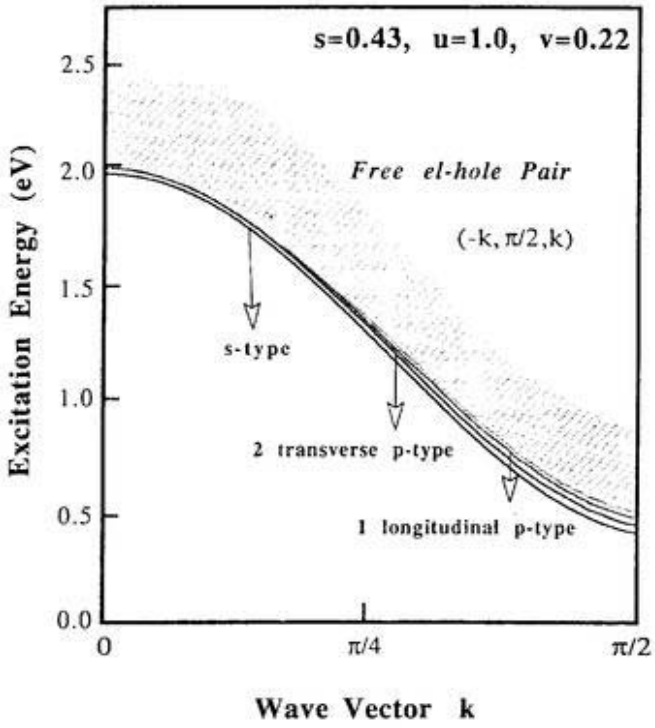

Fig. 4.7. The exciton energy bands of $BaBiO_3$.

4.7 SUMMARY

We have thus studied ground and excited states of the CDW in $BaBiO_3$, using 3-D extended Peierls-Hubbard model. Within this model, we introduce the adiabatic approximation for phonons, and Hartree-Fock approximation for inter electron interactions. The el-hole correlation on the Bi atoms are taken into account so as to obtain the exciton effect. From our calculations we got metallic state with a broad conduction band near the Fermi level. But due to the strong el-ph interaction, this metallic state is unstable, and makes CDW type insulator.

5. LIGHT ABSORPTION SPECTRA OF $BaBiO_3$

5.1 OPTICAL CONDUCTIVITY AND MONTE CARLO SIMULATION

The light absorption spectra in a three-dimensional CDW insulating state are drastically changed by the exciton effect as well as the el-ph interaction. On the other hand, in a vibrating but otherwise perfect crystal, phonons are the natural choice of scatters for the moving electron and hole, and the absorption spectrum is now broadened by this el-ph scattering. This scattering also relaxes the dipole selection rule to various extents, and makes indirect transitions across the insulating gap appear. In order to discuss these characteristics of spectral shape of $BaBiO_3$, we treat the oxygen sub-lattice as classical, because the observed spectra do not show any fine structure which would be related to its quantum nature. Furthermore, the el-ph interaction is considered to be rather strong. The fluctuations of the oxygen sub-lattice coordinates are introduced around the perfect dimerization by using the Monte Carlo (MC) simulation. It is expected that the magnitude of such fluctuations are very sensitive to the el-ph coupling strength s.

As is well known, according to the Franck-Condon principle, only the electronic part of the system is excited, while the phonon part remains fixed at the ground state. Thus, we can calculate the optical conductivity ($\equiv \sigma(\omega)$) according to the Franck-Condon principle as

$$\sigma(\omega) \equiv \frac{1}{\omega} \int \prod_l dq_l W_B(E_g(\{q_l\})) \sum_n \left| J_{n,g} \right|^2 \times \delta(E_n''(q_l) - E_g(q_l) - \hbar\omega). \tag{5.1.1}$$

Here, $J_{n,g}$ is the matrix element between the ground state $|g\rangle$ and the excited state $|n\rangle''$ of the current operator $\hat{J}$, which is defined as

$$\hat{J} \equiv iT' \sum_{\langle l,l' \rangle} \sum_{\sigma} (\vec{e}_{ll'} \cdot \vec{p}) \{ a^{\dagger}_{l\sigma} a_{l'\sigma} - a^{\dagger}_{l'\sigma} a_{l\sigma} \}, \tag{5.1.2}$$

while T' is the dipole transition matrix element, assumed to be independent of l and l'. $\vec{e}_{ll'}$ denotes the unit vector from l to l', and $\vec{p}$ is the unit vector of the polarization of light. ω is the frequency of the incident photon. The Boltzmann factor W_B is defined as

$$W_B(E_g(q_l)) = \frac{\exp(-E_g(q_l)/k_B T^*)}{\int \prod_l dq_l \exp(-E_g(q_l)/k_B T^*)}. \tag{5.1.3}$$

Here, $E_g(q_l)$ is the energy of the ground state, and q_l ($l = 1, \cdots, N$) is the lattice configuration including the lattice fluctuation around the equilibrium position given by the Peierls distortion $\bar{q}_l$. This energy $E_g(q_l)$ is calculated for each configuration q_l within the HF approximation. T^* in eq. (5.1.3) is the effective temperature, which implicitly includes the quantum fluctuation of the phonon. In the semi-classical approximation, T^* should be related to the true temperature T as

$$k_B T^* = \frac{1}{2} \hbar \bar{\omega}_0 \coth\left(\frac{\hbar \bar{\omega}_0}{2 k_B T} \right), \tag{5.1.4}$$

where $\bar{\omega}_0$ is the average frequency of the phonons. $E_n''(q_l)$ in eq. (5.1.1) is the energy of excited state for a given q_l calculated by the same principle as described in eq. (4.3.4). In actual calculations for eq. (5.1.1), the Monte Carlo averaging is performed by the importance sampling [59].

The spectral shapes of $BaBiO_3$ are exotic because the observed spectra exhibit a sharp peak near the visible region ($\approx$2.0 eV), as well as a long absorption tail near the infrared region. Let us now see why we have these two spectral parts. The one-electron energy bands and the density of states of the CDW state, thus calculated, are shown in Figs. 4.4 and 4.5 respectively. From this figure, we can see that the direct gap appears at $W(\equiv XM/2)$ point of the first Brillouin zone with energy $\approx$2.0 eV, while the indirect gap opens up between the X and L $(\equiv \Gamma R/2)$ points with energy $\approx$0.55 eV. Since the strong electron-phonon interaction is acting in this BBO, it causes a Peierls distortion of the lattice, doubling the unit cell, opening up a wide direct gap, and also makes the indirect transition to appear. So, both the direct gap, and the indirect transition have the same origin. In this section, we have study the light absorption spectra at near-infrared and visible regions of BBO.

Since we are going to calculate absorption spectra which take into account the exciton effect as well as lattice fluctuation in this three dimensional BBO system, the whole calculation becomes very complicated. So, for overcoming the difficulties of our numerical calculation, we will consider a lattice that consists of $4\times4\times4$ sites occupied by $4\times4\times4$ electrons, and impose the periodic boundary condition for this cluster, so as to reduce the finite size effects.

5.2.1 DIRECT EXCITON

Here, we calculate the light absorption spectrum under the condition of rigid lattice or without the thermal lattice fluctuation. Under this condition, the

possible optical transitions are always direct ones. By using the ground and excited states that determined according to the principle that mentioned in sections 4.1-4.3, we can calculate the optical conductivity $\sigma(\omega)$ from the following formula

$$\sigma(\omega) \equiv \frac{1}{\omega} \sum_{n} \left| J_{n,g} \right|^2 \delta(E_n'' - E_g - \hbar\omega). \qquad (5.2.2)$$

Figure 5.1(a) shows the Hartree-Fock level spectral shape without exciton effect. Here, the discrete lines correspond to the inter-band transitions, and the gap appears at around 2.0 eV.

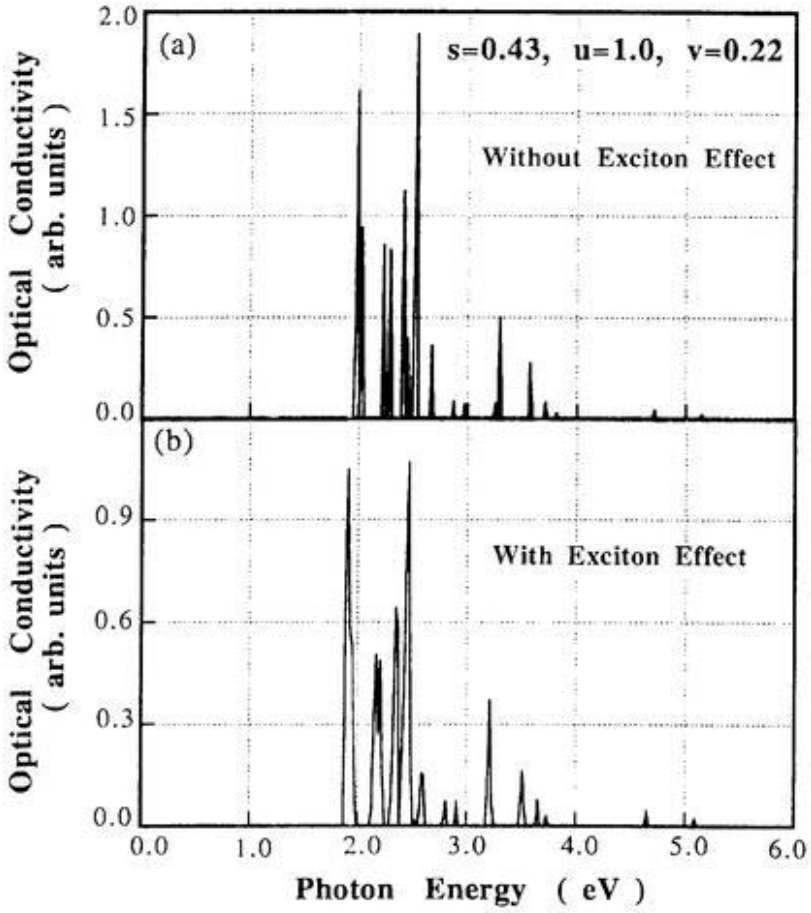

Fig. 5.1. The absorption spectra in the uniform CDW state. s=0.43, u=1.0, v=0.22; (a) Without exciton effect. (b) With exciton effect.

On the other hand, when the exciton effect is taken into account, the spectral shape is modulated, as shown in Fig. 5.1(b). In this case, the largest peak around 1.92 eV is due to the charge transfer type exciton, while the following higher energy peaks are still due to the inter-band transitions.

We can see from this figure, that the oscillator strength of the lowest transition line increased due to the exciton effect, though the exciton binding energy itself is rather small. This exciton binding energy is mainly depends on inter-site Coulomb energy v. Up to now, as far as these spectral shapes are concerned, the absorption in the indirect gap part has no intensity, because of the k-selection rule.

5.2.2 DIRECT AND INDIRECT EXCITONS WITH LATTICE FLUCTUATIONS

Let us now introduce the lattice fluctuations of the oxygen sub-lattice coordinates. At finite temperatures, these coordinates are considered to be fluctuating as classical variables. These fluctuations are taken into account as a Boltzmann distribution around the Peierls distortion q. After introducing this lattice fluctuation, we can determine the ground and excited states. Then we can calculate the optical conductivity according to the principle as described in section 5.1.

Thus we could introduce the lattice fluctuations, and the calculated absorption spectrum in the visible region is shown in Fig. 5.2(b). In this figure, spectra for both with and without exciton effects are also shown. In both cases, we have a broad single absorption band whose peak is at around 2.0 eV. We can also see that, due to the exciton effect, the peak now shifts towards the lower energy side, and its intensity has increased. The calculated absorption spectral shape with the exciton effect also agrees well with the experimental

result [7,26] shown in Fig. 5.2(a). In this calculation, we have set the temperature T=300 K as in the case of experiment. For the average phonon frequency, we set $\overline{\omega}_0$=570 cm^{-1} according to the experiment [28]. By using these T and $\overline{\omega}_0$, the effective temperature becomes T^*=468 K, and this T^* is used for our calculation.

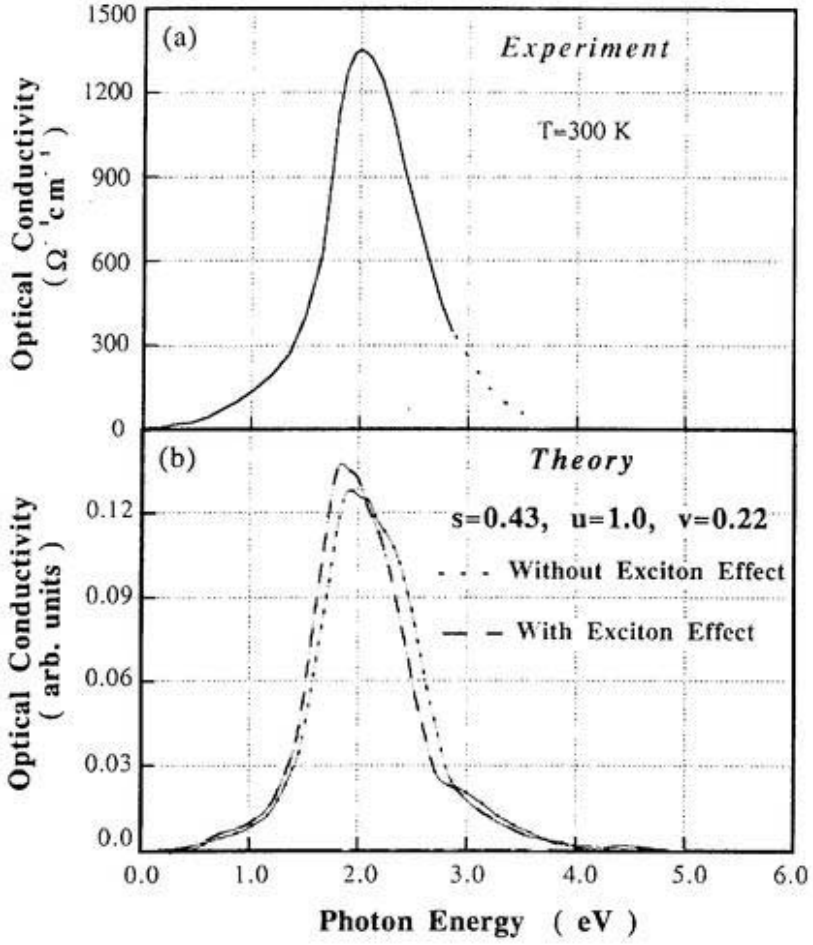

Fig 5.2. The absorption spectrum of BBO in the visible region. (a) Experiment [26]. (b) Present calculation; T^*=468 K.

We have also calculated the light absorption spectrum at near-infrared region which corresponds to the indirect excitation across the CDW gap. Here, due to lattice fluctuations, the k-selection rule is somewhat relaxed and the

indirect transition becomes possible. The calculated absorption spectrum in the infrared region is shown in Fig. 5.3(b). In this figure, spectra for both with and without exciton effects are shown. The result with the exciton effect almost agrees with the experiments [24,25] shown in Fig. 5.3(a). There are small discrepancies between our calculated result and the experimental one at the infrared region. Our calculation is only concerned with the pure electronic transitions, for this reason, the calculated intensity vanishes below 0.2 eV. While, in the case of experiment, there is absorption intensity due to phonon in this region.

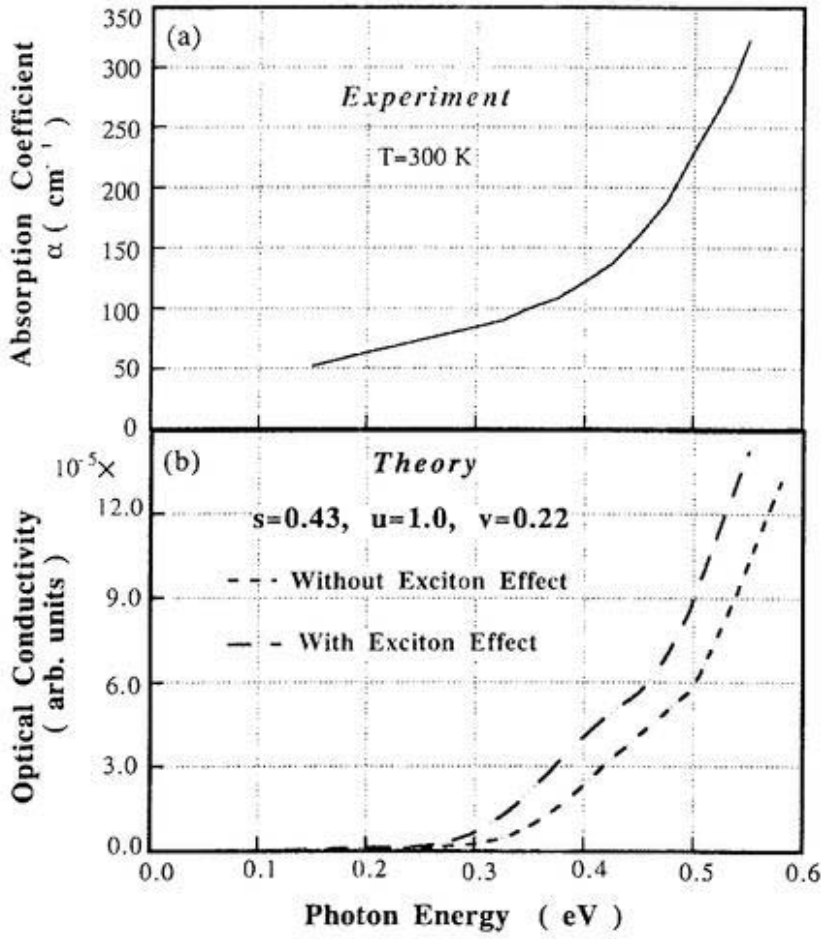

Fig. 5.3. The absorption spectrum of BBO in the near infrared region. (a) Experiment [24]. (b) Present calculation ; T^*=468 K.

The results of our unified theory for both infrared and visible regions are summarized in Fig. 5.4(b), and are compared with the experiment [26] Fig. 5.4(a). In Fig. 5.4(b), the discrete lines are the theoretical absorption spectrum without lattice fluctuations, while the dotted gray curve is with lattice fluctuations.

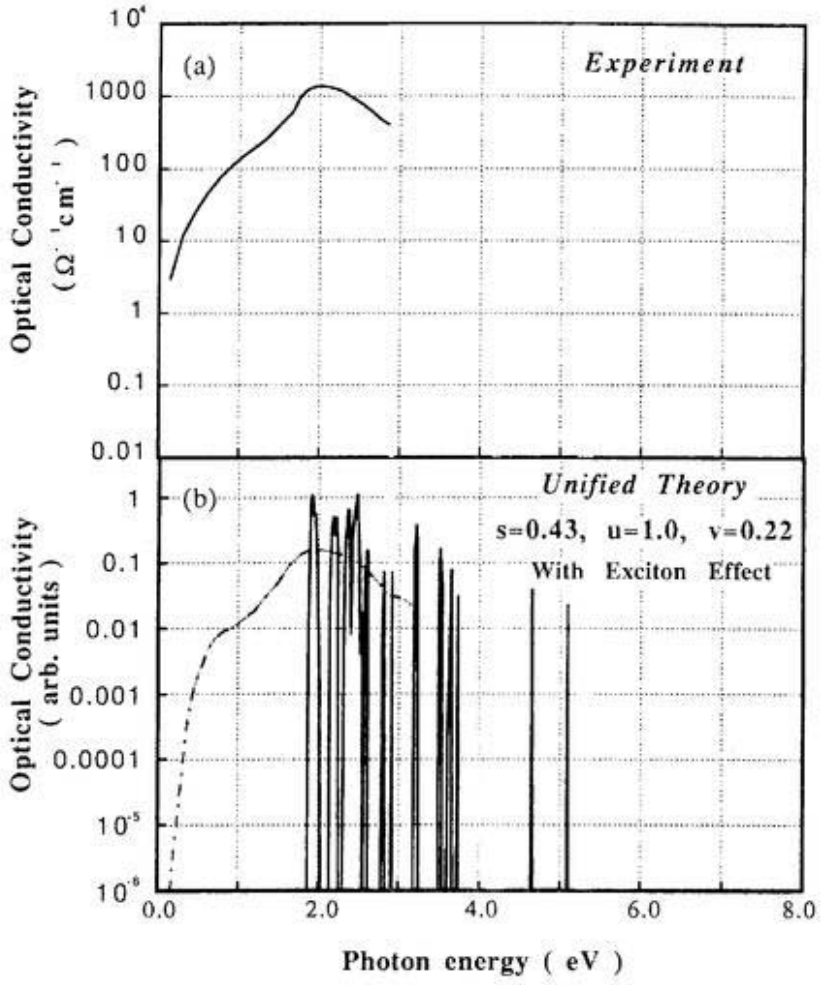

Fig 5.4. The absorption spectrum of $BaBiO_3$ from the infrared to the visible regions, (a) Experiment [26]. (b) Present calculation; T^*=468 K.

To make the agreement between the theory and the experiment more transparent, we can roughly compare the spectral intensity ratios between the

near infrared and the visible regions for both cases. From our calculated results, we can estimate this ratio ($\equiv R_c$) in the following way. The spectral intensity at the peak of the visible region of absorption spectrum ($\equiv I_{vis}$) is 0.138 (arb. unit), while the near infrared intensity ($\equiv I_{\inf}$) at the energy 0.3 eV is about 0.78×10^{-5} (arb. unit). Therefore, the intensity ratio $R_c(\equiv I_{\inf} / I_{vis})$ is 5.6×10^{-5}. In the same way, we can calculate the intensity ratio ($\equiv R_e$) from the experimental results, and it becomes 4.79×10^{-5}. This, experimental value agrees well with the calculated one.

5.3 SUMMARY

We have thus theoretically studied the optical properties of $BaBiO_3$, in connection with the direct and indirect excitons. Within our unified theoretical model, the near-infrared and visible absorption spectra of BBO are clarified from a unified point of view. It is shown here that the two distinct absorption spectra of the optical transitions occur due to the direct and indirect excitations. The direct transition corresponds to the excitation across the direct CDW gap, and this gap arises due to the frozen part of the Peierls distortion. While the indirect part corresponds to the long tail in the infrared region of the absorption spectrum, and it is due to the excitation across the indirect CDW gap. It arises due to the lattice fluctuations from the static Peierls distortion. This lattice fluctuation relaxes the k-selection rule, and makes the indirect transition possible. It also shown that due to exciton effect the distribution of the oscillator strength changes drastically, though the exciton binding energy itself is rather small. These results are in good agreements with experiments.

6. NONLINEAR LATTICE RELAXATION OF CHARGE TRANSFER EXCITONS IN $BaBiO_3$

6.1 THEORY AND CALCULATION FOR LATTICE RELAXATION

In the previous chapter, we have studied the optical properties as well as the band dispersion of $BaBiO_3$. We found that the appearance of direct and indirect gaps are due to the characteristic and complicated nature of the one electron energy band $E(k)$ around the Fermi level. Because, in the case of three-dimensional metal oxides, the one-body energy $E(k)$ of the electron around the Fermi level is usually a complicated function of k. It depends on the nature of three-dimensional chemical bonds among the s-orbital of the metallic atoms and the three p-orbitals of O's. As a result, it often occurs that even after the CDW type metal-insulator transition, optical excitations appear below the CDW gap. In this case, we have a *mid-gap absorption*, which is not due to the collective excitations in the gap such as *solitons*, but simply due to the complicated k-dependency of the one-electron energy band. Recently, this type of low energy optical excitation is found below the CDW gap of BBO [33-37].

On the other hand, several new reflectivity peaks appears around the midgap energy in the photo-induced reflectance measurements [33] of $BaBiO_3$. This indicates the evidence for a lattice relaxation after removing electrons from the valence band and as a consequence energy levels appear within the gap .

Let us now consider the nonlinear lattice relaxation of the exciton in this three-dimensional CDW type material $BaBiO_3$. To describe the relaxation path from the free exciton to the *self-trapped exciton* (STE), we use the following variational function for q_l

$$q_l = (-1)^l q\{1 + \Delta q[\tanh\theta(|l| - l_0/2) - 1]\}, \qquad (6.1.1)$$

where, $(-1)^l q$ denotes the Peierls distortion in the CDW ground state, and this q should be determined beforehand within the HF approximation. The curly bracket denotes the local lattice displacement from this ground state. Δq is its amplitude and $[\cdots]$ denotes its pattern. θ corresponds to the reciprocal width of the distortion. l $(\equiv l_x, l_y, l_z)$ is a vector which expresses the lattice points in a three-dimensional cubic lattice. l_0 is the length of the cubic distortion.

Using this q_l, we can determine the energies of the ground and excited state as well as their wave function according to the theories of Sects. 4.1 and 4.2. As for the excited state, we take into account the correction for the h^{HF} by the principle which already mentioned in Sect. 4.3.

In Figs. 6.1 and 6.2, we have shown the potential surfaces in the ground state and the first excited state, respectively. Here, each surface is drawn in the two dimensional space spanned by l_0 and Δq, and being optimized for θ in each state. In Fig. 6.2, the point at l_0=2.1 and Δq=0.7 corresponds to the self-trapped exciton. All the energies are referenced from the energy of the ground state of CDW, and this notation will be used hereafter.

Fig. 6.3 shows the charge density distribution of CDW ground state, and this is entirely same as in Fig. 4.6. The new charge density attained by the creation of relaxed excited state is shown in Fig. 6.4. The difference between these two is shown in Fig. 6.5, as well. The charge density of the ground state and that of the STE state along the x axis are also shown in Fig. 6.6, and its lower part shows difference between them. The arrow shows the center of distortion.

This self-trapped state partially cancelled the charge density distribution of the uniform CDW ground state, and it returned back towards the metallic state.

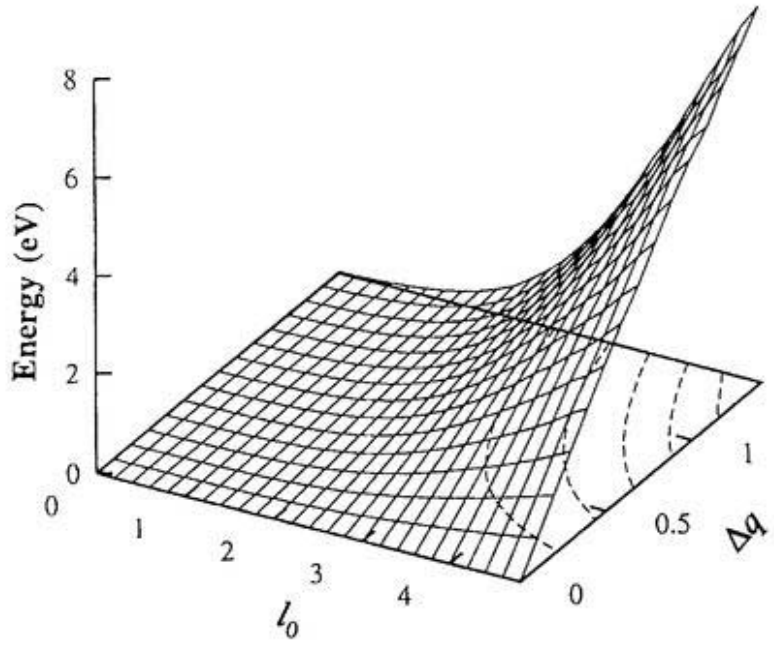

Fig. 6.1. The potential surface in the ground state.

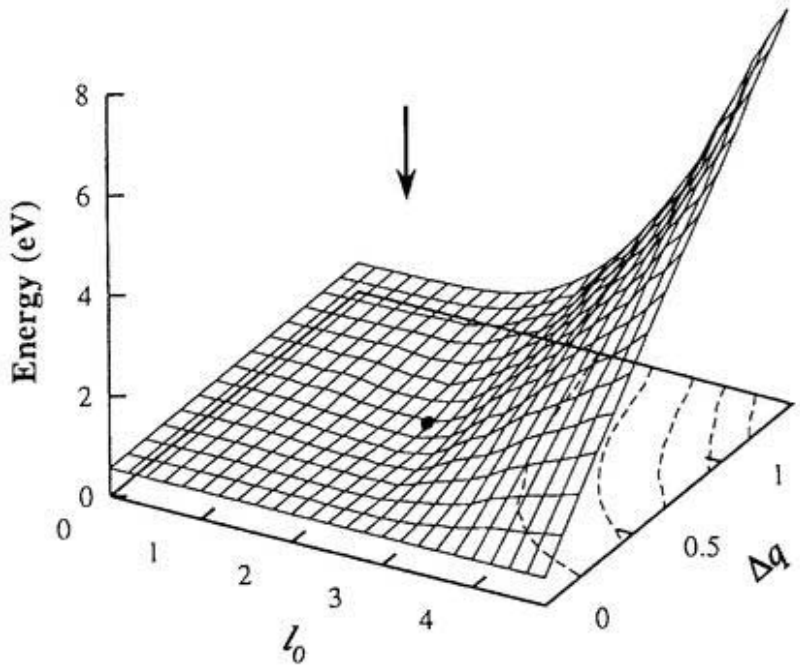

Fig. 6.2. The potential surface in the first excited state.

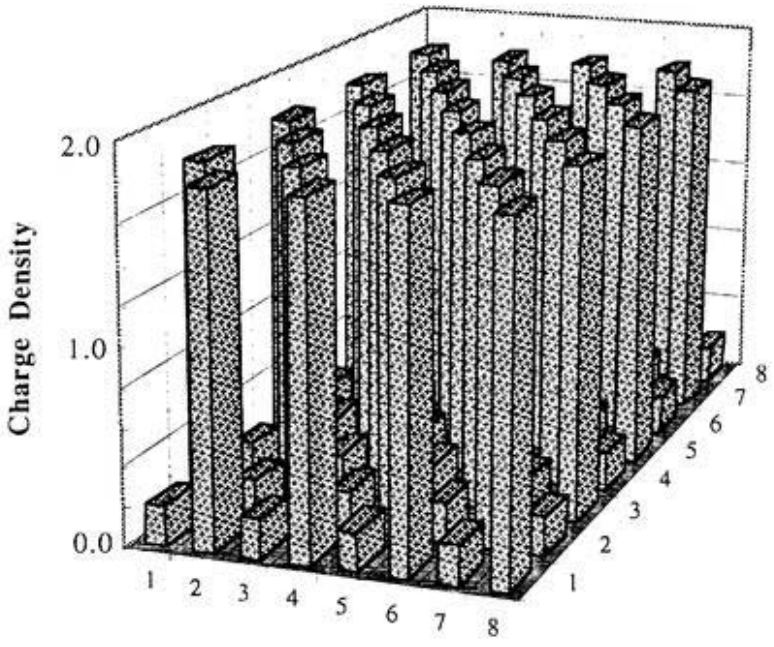

Fig. 6.3. The charge density of a CDW ground state. On a 8×8 plane.

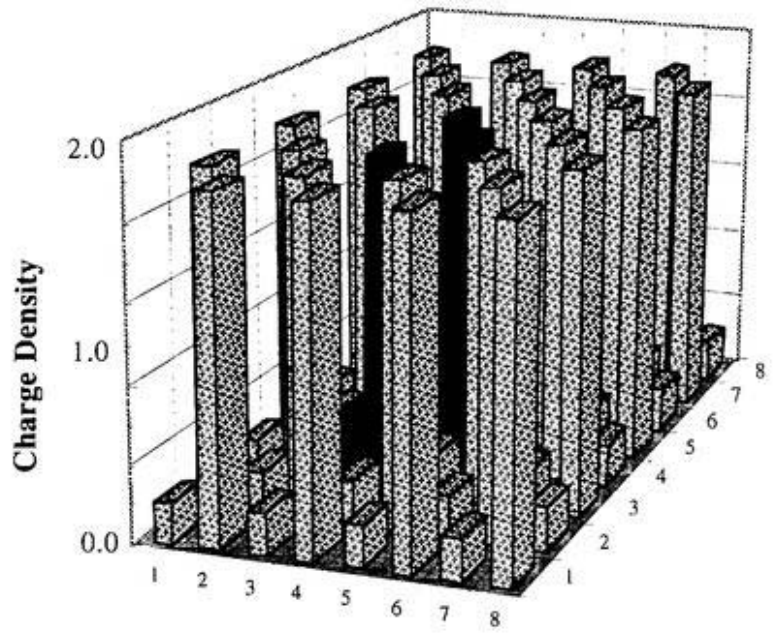

Fig. 6.4. The charge density around the relaxed excited state. On a 8×8 plane.

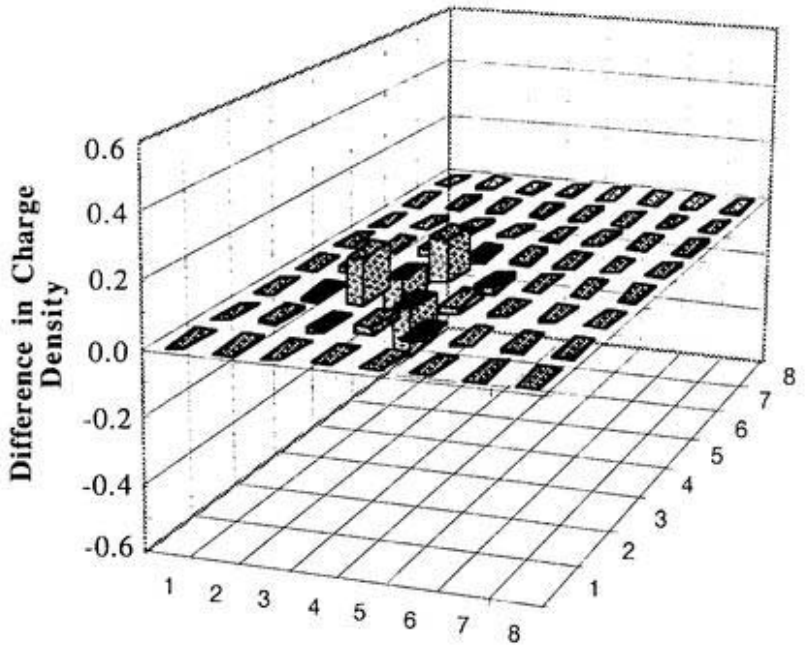

Fig. 6.5. Difference of charge density between the relaxed excited state and the uniform CDW. On a 8×8 plane is shown.

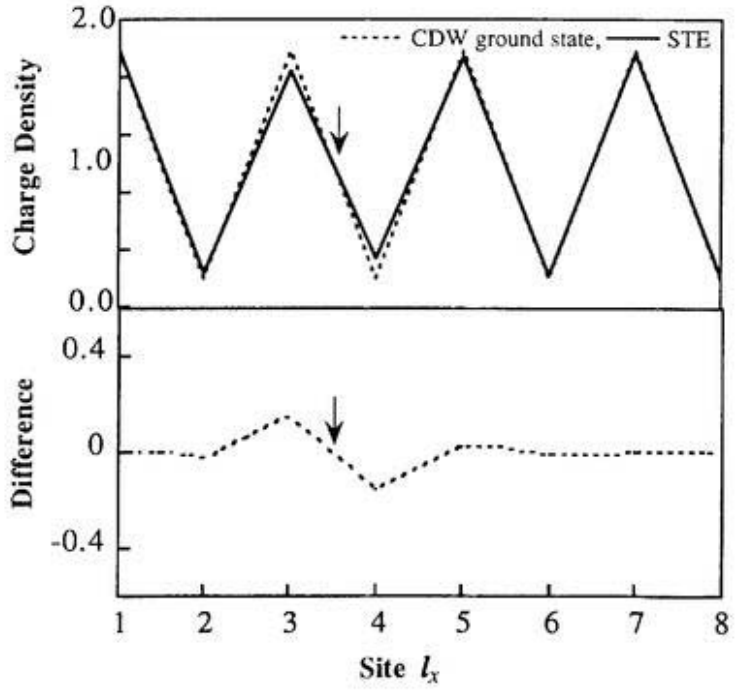

Fig. 6.6. Charge density of CDW ground state and STE state are plotted as a function of l_x, the lower panel shows their difference.

Our aim in this section, is to clarify the lattice relaxation paths of the photogenerated CT exciton and the main origin of the photoinduced absorption band, as mentioned in Sect. 3.2 at the energy range 0.7~0.9 eV. The numerical results for the adiabatic potential energy along the relaxation path of the exciton is shown in Fig. 6.7 as a function of l_0. Δq and θ are determined to minimize E_{x_1}.

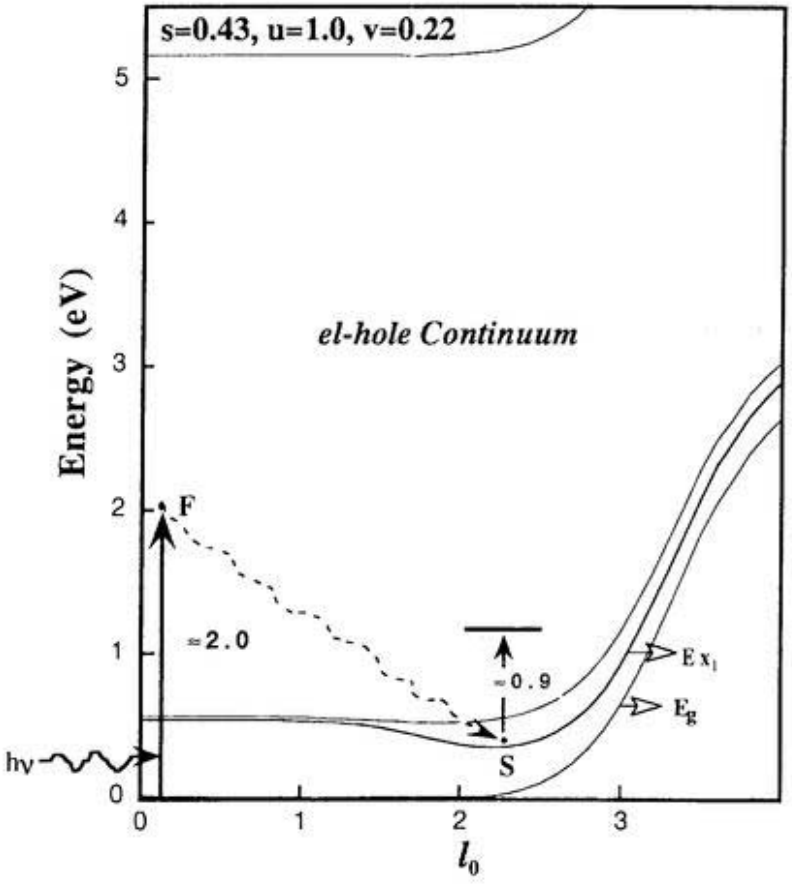

Fig. 6.7. Adiabatic potential energy surface from the CT exciton to the self trapped exciton as a function of l_0.

The physical interpretation of this relaxation path are as follows. When

electrons are removed by photoexcitation, the CDW is locally destroyed. That is, the electron induces a new local lattice distortion around itself (~ polaron), and gives a localized state. In this localized state the electron is self-trapped, and as a consequence, an energy level appears within the gap, as marked by S in Fig. 6.7. This energy level could be observed in the photoinduced absorption measurement. The optical transition relevant to this absorption will be from this localized state in the gap (STE) to the peak of the density of states of the conduction band, as shown in Figs. 6.7 and 6.8. It is expected to be ~0.9 eV. The photoinduced reflectivity peaks at around mid-gap energy ($h\nu \approx 0.88$ eV) which is shown in Fig. 3.4 [33], can be interpreted as due to this STE.

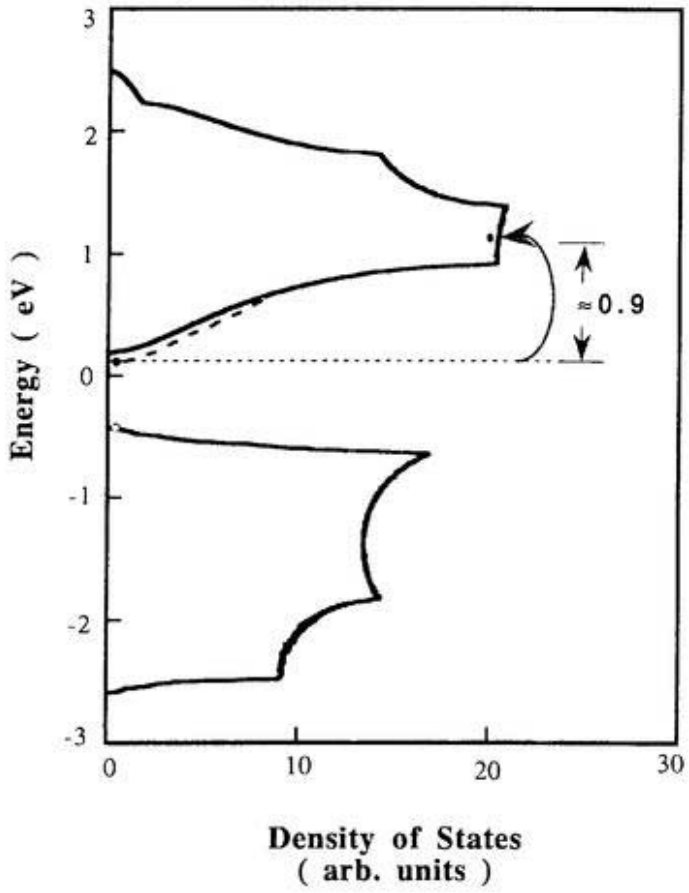

Fig. 6.8. The density of states of CDW, and explanation of photoinduced absorption.

6.3. SUMMARY

We have studied the ground and excited states of the three-dimensional extended Peierls-Hubbard model with half-filled band electrons, so as to clarify the origin of the photoinduced absorption of CDW in $BaBiO_3$. The charge transfer (CT) exciton is created by removing the electron from the valence band by the incident photon with higher energies than its threshold energy. However, due to the local lattice distortion this electron is self-trapped. The experimentally observed photoinduced reflectivity peaks at around mid-gap energy is assigned for the optical excitation from this localized state (STE) to the peak of the density of states of the conduction band.

7. DISCUSSIONS

We have thus theoretically studied the electronic and optical properties of $BaBiO_3$, as one of the typical material with three dimensional CDW state, in connection with nonlinear excitations. The ground and excited states of a three dimensional extended Peierls-Hubbard model with half-filled band electrons have been evaluated. Within this model, we introduce the adiabatic approximation for phonons, and the Hartree-Fock approximation for inter-electron coulombic interactions. The electron-hole correlation on the Bi atoms and the classical fluctuations of the oxygen sub-lattice coordinates are also taken into account, to obtain exciton effect as well as thermal fluctuations of the lattice.

It is well known that, two types of gap exist in this CDW type insulator $BaBiO_3$, one is direct and the other is indirect. In usual insulators, however, the opening of optical gap (direct gap) and the appearances of indirect gap are often considered separately. The optical gap usually comes from the difference between the occupied and unoccupied atomic orbitals relevant to the valence and the conduction bands. While the indirect transition usually appears because of the weak electron phonon coupling, which slightly mixes up direct and indirect transitions.

On the other hand, BBO is not an ordinary insulator, a strong electron-phonon interaction is acting in this material, which causes a Peierls distortion of the lattice, doubles the unit cell, opens up a wide direct gap, and makes the indirect transitions to appear. So both the direct gap and the appearance of the indirect transition have the same origin. For this reason, in our theory, we did not use the conventional perturbation approach, instead, we have developed a unified theory based on the extended Peierls-Hubbard model.

In our study, we assumed that our system is phonon mediated, and the main property arises due to this electron-phonon coupling. Perhaps the most important aspect of our treatment is the unified theory, that we have provided for the occurrence of two gaps in the insulating phase of the barium bismuthates. This picture with the two gaps is consistent with the fact that the indirect gap is not directly accessible in the optical measurements. However, optical experiments must be able to see this, as a phonon assisted transition. Indeed, by fitting the theoretical gaps to the experimental ones, we have estimated the interaction parameters (s, u and v) as well as the transfer energies (T_1, T_2, T_3 and T_4) of the system. With these parameter values we have calculated the CDW ground state itself, optical properties, and as for as the nonlinear lattice relaxation process of exciton. Our theory is unified theory, in that sense that throughout our calculation, we used only a set of fitting parameter values which gives best fitting for the experiments.

By using our model, we at first clarified the near infrared and visible absorption spectra of BBO from a unified point of view. The direct transition corresponds to the excitation across the direct CDW gap, and this gap arises due to the frozen part of the Peierls distortion. While the indirect part corresponds to the long tail in the infrared region of the absorption spectrum, and it is due to the excitation across the indirect CDW gap. It arises due to the lattice fluctuations from the static Peierls distortion. This lattice fluctuation destroys the k-selection rule, and makes the indirect transition possible. Our result shows that, the origin of both the direct gap and indirect transitions are the same, i.e., the strong coupling between the electron and the breathing motion of the oxygen atom. It also shown that due to exciton effect the distribution of the oscillator strength changes drastically, though the exciton

binding energy itself is rather small. These theoretical results show good agreement with recent optical experiments on BBO.

Next, we have studied the nonlinear lattice relaxation process of exciton, and explained the origin of the photoinduced absorption in $BaBiO_3$. The adiabatic potential energy surfaces, that describe the nonlinear relaxation from the Franck-Condon state to the STE, have been calculated within our unified theory. When the CT excitation is created by its threshold energy, the exciton relaxes down to a STE, and localizes within the CDW gap. This localized self-trapped state partially cancelled the charge density distribution of the uniform CDW ground state, and returns back towards the metallic state. It will give a new absorption band with an energy of about a half of the energy gap. This energy level could be observed in the photoinduced absorption measurement. The experimentally observed photoinduced reflectivity peak at around mid-gap energy is assigned for the optical excitation from this localized state (STE) to the peak of the density of states of the conduction band.

Let us briefly discuss these nonlinear excitations from a somewhat different point of view. The collective excited states described in this work can never be created by ordinary thermal excitations from the ground state, because a much larger energy is required than the ordinary thermal energy such as at room temperature. It becomes possible only when the energy is supplied by photoexcitation. That is, as a combination of the photoexcitation and the subsequent lattice relaxations, we can clarify the multistable nature of the ground state, even when thermal excitations can never access it.

8. CONCLUSIONS

In this and preceding chapters, we have investigated the extended Peierls-Hubbard model, as a model to the $BaBiO_3$ with half-filled band electrons. From our study the following results have been worked out.

In our calculations, without el-ph interaction, this material shows metallic state with a broad conduction band, at the center of which, the Fermi level is. However, due to the strong el-ph interaction, this metallic state becomes unstable, and changes into the CDW type insulator. In this CDW insulator, we got two gaps, one of them is direct gap and the other is indirect one.

The light absorption spectra based on our unified theoretical model can explain both the direct and indirect optical transitions. The direct transition corresponds to the excitation across the direct CDW gap, and arises due to the frozen part of the Peierls distortion. While the indirect part corresponds to the long tail in the infrared region of the absorption spectrum and arises due to the lattice fluctuations therefrom. So, our conclusion is that, the origin of both the direct gap and indirect transitions are the same, i.e., the strong coupling between the electron and the breathing motion of the oxygen atom. Also, the exciton effect plays an important role in the absorption spectrum. It is shown that due to exciton effect the distribution of the oscillator strength changes drastically, though the exciton binding energy itself is rather small. These results are in good agreement with experiments.

Our result also indicates the evidence for lattice relaxation of exciton. When the CT excitation is created by its threshold energy, the exciton relaxes down to a STE, and localizes within the CDW gap. This localized self-trapped state partially cancelled the charge density distribution of the uniform CDW ground state, and returns back towards the metallic state. It will give a new

absorption band with an energy of about a half of the energy gap. This energy level could be observed in the photoinduced absorption measurement. The experimentally observed photoinduced reflectivity peak at around mid-gap energy is assigned for the optical excitation from this localized state (STE) to the peak of the density of states of the conduction band.

9. FUTURE PROSPECT

In this BBO systems, both the magnetism and the strong inter-electron coulombic correlation are absent, and so, it is necessary for us to determine whether the superconductivity of BKBO is due to the electron-phonon mechanism only, or if another mechanism is at work. Many studies suggested that superconductivity in BKBO is well described by the Bardeen-Cooper-Schrieffer (BCS) theory, with the electron-phonon interaction playing the key role in the pairing. As is well known, the role of phonons in superconductivity is typically established by the isotope effect, and the existence of isotope effect in the present BKBO and BPBO have been reported in the literatures [48,49,60]. This clearly shows that phonons are involved in the superconductivity. So far there has been no fully successful theoretical treatment of these systems for all ranges of doping. In future, we are planning to extend our theory to explain the doping dependence $BaBiO_3$ systems.

Acknowledgments

I would like to express a deep sense of gratitude to my academic advisor Professor Keiichiro Nasu, who given me the opportunity for study in Japan. With his constant encouragement's, kind supervision and many valuable suggestions for my studies make this works to completion. I shall remain ever grateful to him. I would also like to thank Professor H. Uwe and Dr. K. Iwano for valuable discussion. My great appreciation is also extend to Professor M. Ando, who gave me some good suggestions about the writing of this thesis. I thank Dr. N. Tomita and Dr. T. Minami for helpful advice on the methods of numerical calculations. I would like to acknowledge that this work is a natural extension of Dr. A. Z. Chowdhury's Ph. D thesis [61]. The knowledge found there has been helpful for me.

Finally, I wish to record my indebtedness to all of my family members.

References

[1]. J. G. Bednorz and K. A. Müller, *Z. Phys.* **B 64**, 189 (1986).

[2]. A. W. Sleight, J. L. Gillson and P. E. Bierstedit, *Solid State Commun.* **17**, 27 (1975).

[3]. L. F. Mattheiss, E. M. Gyorgy and D. W. Johnson, Jr., *Phys. Rev.* **B 37**, 3745 (1988).

[4]. L. F. Matteiss and D. R. Hamann, *Phys, Rev.* **B 26**, 2686 (1982); **28**, 4227 (1983).

[5]. N. Hamada, S. Massida, A. J. Freeman and J. Redinger, *Phys. Rev.* **B 40**, 4442 (1989).

[6]. D. A. Papaconstantopoulos, A. Pasturel, J. P. Julien and F. Cyrot Lackmann, *Phys. Rev.* **B 40**, 8844 (1989).

[7]. S. Tajima, S. Uchida, A. Masaki, H. Takagi, K. Kitazawa, S. Tanaka and S. Sugai, *Phys. Rev.* **B 35**, 696 (1987).

[8]. C. M. Varma, *Phys. Rev. Lett.* **61**, 2713 (1988).

[9]. R. D. Shannon, *Acta Crystallogr.* **A 32**, 751 (1976).

[10]. Ricardo P. S. M. Lobo and Francois Gervais, *Phys. Rev.* **B 52**, 13294 (1995- II).

[11]. H. Sato, S. Tajima, H. Takagi and S. Uchida, *Nature* **338**, 241 (1989).

[12]. D. E. Cox and A. W. Sleight, *Solid State Commun.* **19**, 969 (1976).

[13]. G. Thornton and A. J. Jacobson, *Acta Crystallogr.* **B 34**, 351 (1978).

[14]. T. M. Rice and L. Sneddon, *Phys. Rev. Lett.* **47**, 689 (1981); *Physica* **107B**, 661 (1981).

[15]. E. Jurczek and T. M. Rice, *Europhys. Lett.* **1**, 225 (1986).

[16]. D. Yoshioka and H. Fukuyama, *J. Phys. Soc. Jpn.* **54**, 2996 (1985).

[17]. G. Vielsack and W. Weber, *Phys. Rev.* **B 54**, 6614 (1996-I).

[18]. Y. Koyama and M. Ishimara, *Phys. Rev.* **B 45**, 9966 (1992).

[19]. H. Minami, *Physica* **C185-187**, 1257 (1991).

[20]. K. Takegahara and T. Kasuya, *J. Phys. Soc. Jpn.* **56**, 1478 (1987).

[21]. A. I. Liechtenstein, I. I. Mazin, C. O. Rodriguez, O. Jepsen and O. K. Andersen, *Phys. Rev.* **B 44**, 5388 (1991).

[22]. J. B. Boyce, F. G. Bridges, T. Claeson, T. H. Geballe, G. G. Li and A. W. Sleight, *Phys. Rev.* **B 44**, 6961 (1991).

[23]. H. Namatame, A. Fujimori, H. Takagi, S. Uchida, F. M. F. deGroot and J. C. Fuggle, *Phys. Rev.* **B 48**, 16917 (1993).

[24]. H. Uwe and K. Tachibana, in *Advances in Superconductivity VII,* edited by K. Yamafuji and T. Morishita (Springer-Verlag, Tokyo, 1995), p. 165.

[25]. M. E. Kozlov, Xiaoli Ji, H. Minami and H. Uwe, *Phys. Rev.* **B 56**, 12211 (1997).

[26]. S. H. Blanton, R. T. Collins, K. H. Kelleher, L. D. Rotter, Z. Schlesinger, D. G. Hinks and Y. Zheng, *Phys. Rev.* **B 47**, 996 (1993).

[27]. K. H. Kim, C. U. Jung, T. W. Noh and S. C. Kim, *Phys. Rev.* **B 55**, 15393 (1997).

[28]. S. Sugai, S. Uchida, K. Kitazawa, S. Tanaka and A. Katsui, *Phys. Rev. Lett.* **55**, 426 (1985).

[29]. S. Sugai, *Solid State Commun.* **72**, 1187 (1989).

[30]. B. Batlog, R. J. Cava, L. W. Rupp Jr., G. P. Espinosa, J. J. Kajewski, W. F. Peck and A. S. Cooper, *Physica* **C162-164**, 1393 (1989a).

[31]. A. Inoue, A. Iyo, H. Uwe, T. Sakudo, Y. Tanaka and M. Tokumoto, in *Proc. of 4th Internat. Symp. Superconduct.* (ISS' 91) Tokyo, 139 (1991).

[32]. C. Kittle, *Introduction to Solid State Physics*, Sixth Edition (John Wiely & Sons, Inc.), p. 185.

[33]. W. Markowitsch, V. Schlosser, W. Lang, K. Remschnig and P. Pogl, *Physica* **C 185-189**, 995 (1991).

[34]. X. Wei, A. J. Pal, L. Chen, G. Ruani, C. Taliani, Z. V. Vardeny and R. Zamboni, *Solid State Commun.* **81**, 419 (1992).

[35]. J. F. Federici, B. I. Greene, E. H. Hartford and E. S. Hellman, *Phys. Rev.* **B 42**, 923 (1990).

[36]. G. Ruani, A. J. Pal, C. Taliani and R. Zamboni, in *Proceedings of the 3rd National Meeting on High Temperature Superconductivity*, edited by C. Ferdeghini and A. S. Siri (World Scientific, Singapore), p. 164.

[37]. C. Taliani, A. J. Pal, G. Ruani, A. J. Pal, R. Zamboni, X Wei and Z. D. Vardeny, *Electronic properties of High Tc Superconductors and Related Compounds,* edited by H. Kuzmany, M. Mehring and J. Fink p. 164.

[38]. S. Pei, J. D. Jorgensen, B. Dabrowski, D. G. Hinks, D. R. Richards, A. W. Mitchell, J. M. Newsam, S. K. Sinha, D. Vaknin and A. J. Jacobson, *Phys. Rev.* **B 41**, 4126 (1990).

[39]. A. Taraphder, Rahul Pandit, H. R. Krishnamurthy and T. V. Ramakrishnan *Int. Journal of Modern Physics* **B 10**, 863 (1996); A. Taraphder, H. R. Krishnamurthy, R. Pandit and T. V. Ramakrishnan, *Phys. Rev.* **B 52**, 1368 (1995).

[40]. J. TH. W. De Hair and G. Blasse, *Solid State Commun.* **12**, 727 (1971).

[41]. R. Scholder, K. Ganter, H. Glaser and G. Merz, *Z. Anorg. Allgem. Chem.* **319**, 37(1963).

[42]. S. Pei, N. J. Zalusec, J. D. Jorgensen, D. G. Hinks, A. W. Mitchell and D. R. Richards, *Phys. Rev.* **B 39**, 811 (1989).

[43]. A. W. Sleight, in Chemistry of Oxide Superconductors, ed. C. N. Rao (Black-well Scientific Publications, Oxford, 1988), p. 27.

[44]. S. Pei, J. D. Jorgensen, D. G. Hinks, B. Dabrowski, D. R. Richards, A. W. Mitchell, Y. Zheng, J. M. Newsam, S. K. Sinha, D. Vaknin and A. J. Jacobson, *Physica* **C 162-164**, 556 (1989);
D. T. Marx *et al.*, *Phys. Rev.* **B 46**, 1144 (1993).

[45]. S. Uchida, K. Kitazawa and S. Tanaka, *Phase Trans.* **8**, 95 (1987).

[46]. D. G. Hinks, B. Dabrowski, J. D. Jorgensen, A. W. Mitchell, D. R. Richards, S. Pei and D. Shi, *Nature* **333**, 836 (1988).

[47]. R. J. Cava, B. Batlogg, G. P. Espinoza, A. P. Ramirez, J. J. Kajewski, W. F. Peck Jr., L. W. Rupp jr. and A. S. Cooper, *Nature* **339**, L291 (1989).

[48]. D. G. Hinks, D. R. Richards, B. Dabrowski, D. T. Marx and A. W. Mitchell, *Nature* **335**, 419 (1988).

[49]. B. Batlogg, R. J. Cava, L. W. Rupp jr., A. M. Mujsee, J. J. Kajewski, J. P. Remeika, W. F. Peck Jr., A. S. Cooper and G. P. Espinoza, *Phys. Rev. Lett.* **61**, 1670 (1988).

[50]. L. F. Mattheiss and D. R. Hamann, *Phys, Rev. Lett.* **60**, 2681 (1988).

[51]. K. Iwano and K. Nasu, *Phys. Rev.* **B 57**, 6957 (1998).

[52]. M. Yamashita, Y. Nonaka, S. Kida, Y. Hamaue and R. Aoki, *Inorg. Chem. Acta.* **52**, 43 (1981).

[53]. Masato Suzuki and Keiichiro Nasu, *Synthetic Metals* **64**, 247 (1994).

[54]. K. Nasu, *J. Phys. Soc. Jpn.* **52**, 3865 (1983); **53**, 302 (1984); **53**, 427 (1984).

[55]. Y. Wada, T. Mitani, M. Yamashita and T. Koda, *J. Phys. Soc. Jpn.* **54**, 3143 (1985).

[56]. N. Kuroda, M. Sakai, Y. Nishina, M. Tanaka and S. Kurita, *Phys. Rev. Lett.* **58**, 2122 (1987).

[57]. S. Kurita, M. Haruki and K. Miyanaga, *J. Phys. Soc. Jpn.* **57**, 1789 (1988).

[58]. M. Haruki and S. Kurita, *Phys. Rev.* **B 39**, 5706 (1989).

[59]. N. Metropolis, A. W. Rosenbluth, M. N. Rosenbluth, A. H. Teller and E. Teller, *J. Chem. Phys.* **21**, 1087 (1953).

[60]. H. C. zur Loye, K. J. Leary, S. W. Keller, W. K. Ham, T. A. Faltens, J. N. Michaels and A. M. Stacy, *Science* **238**, 1558 (1987).

[61]. A. Z. Chowdhury, Ph. D thesis, The Graduate University for Advanced Studies, Hayama, Japan, No. kou-173 (1996).